SAND2019-14116PE

# Molecular Simulation of Nanoparticle-Nanopore Interactions: Adsorption, Aggregation and Fracture

**Louise Criscenti**
Geochemistry Department
Sandia National Laboratories
Albuquerque, NM 87185

Built on LDRD Laboratory Directed Research and Development

U.S. DEPARTMENT OF ENERGY | Office of Science

Sandia National Laboratories is a multimission laboratory managed and operated by National Technology and Engineering Solutions of Sandia LLC, a wholly owned subsidiary of Honeywell International Inc. for the U.S. Department of Energy's National Nuclear Security Administration under contract DE-NA0003525.

# Sandia's History

*Exceptional service in the national interest*

- July 1945: Los Alamos creates Z Division
- Nonnuclear component engineering
- November 1, 1949: Sandia Laboratory established

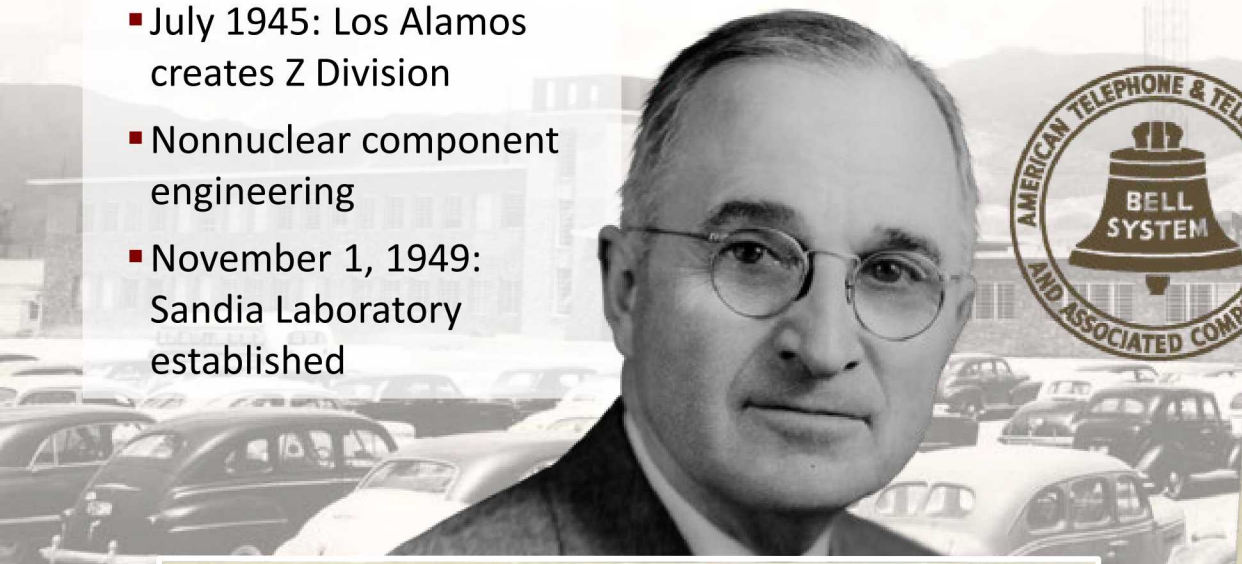

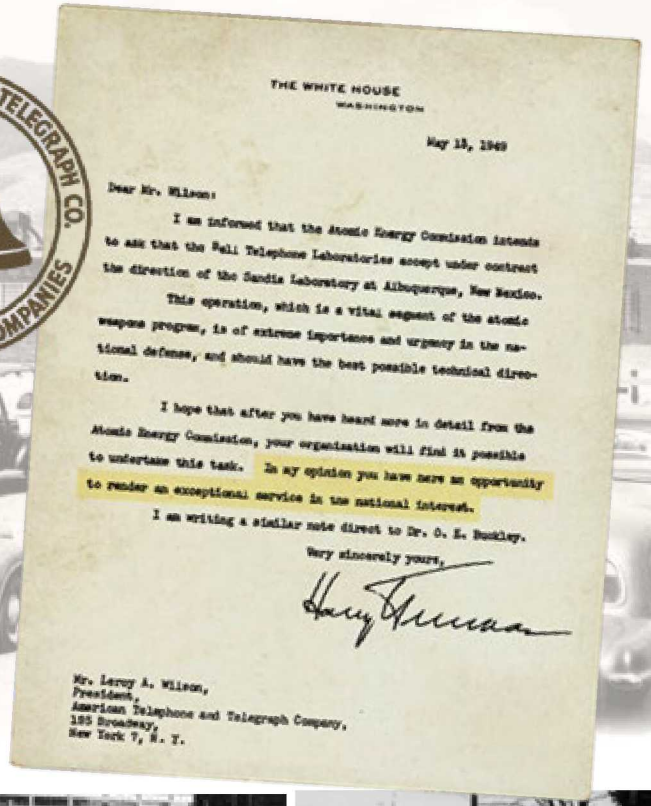

THE WHITE HOUSE
WASHINGTON

May 13, 1949

Dear Mr. Wilson:

I am informed that the Atomic Energy Commission intends to ask that the Bell Telephone Laboratories accept under contract the direction of the Sandia Laboratory at Albuquerque, New Mexico.

This operation, which is a vital segment of the atomic weapons program, is of extreme importance and urgency in the national defense, and should have the best possible technical direction.

I hope that after you have heard more in detail from the Atomic Energy Commission, your organization will find it possible to undertake this task. In my opinion you have here an opportunity to render an exceptional service in the national interest.

I am writing a similar note direct to Dr. O. E. Buckley.

Very sincerely yours,

Harry Truman

Mr. Leroy A. Wilson,
President,
American Telephone and Telegraph Company,
195 Broadway,
New York 7, N. Y.

to undertake this task. In my opinion you have here an opportunity to render an exceptional service in the national interest.


# Sandia National Laboratories Highlights


## Sandia Mission Focus

- Nuclear Deterrence
- National Security Programs
- Integrated Security Systems (Energy, Climate)
- Defense Nuclear Nonproliferation
- Advanced Science & Technology

**Government-owned, contractor-operated**
**Federally funded research and development center**


**Six sites – NM, TX, CA, NV, HI**

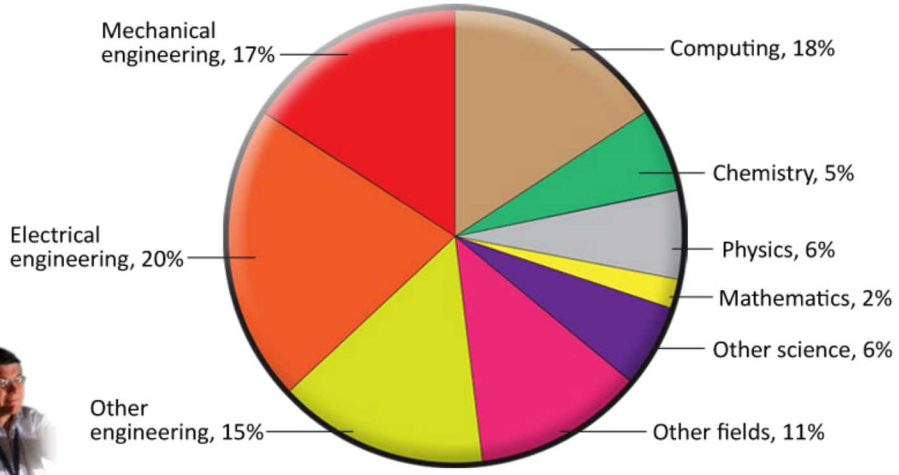


**~11,000 employees, ~5000 technical staff**

# Sandia Program Portfolios

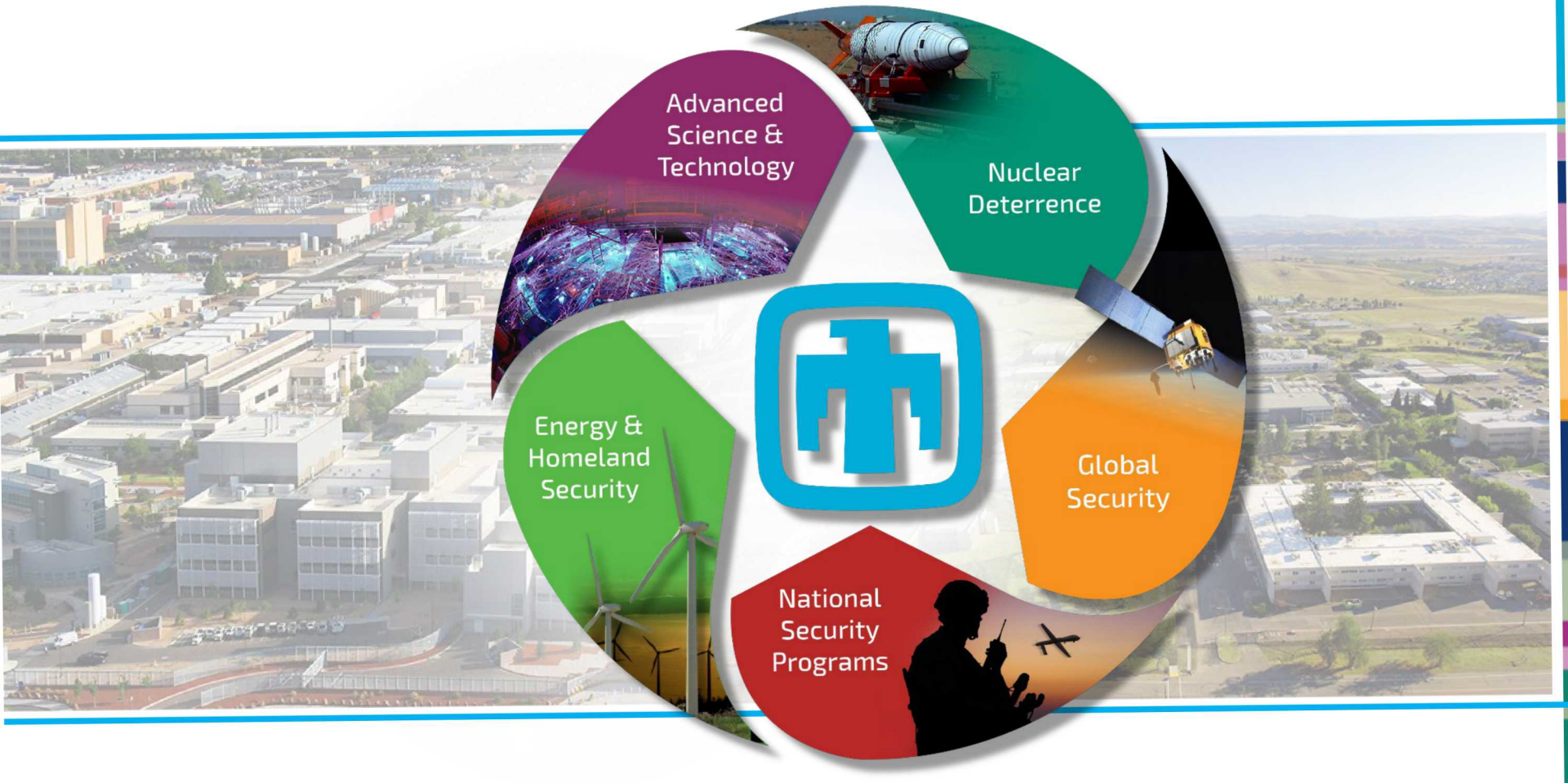

# Geochemistry Department

- Experimental geochemistry
- Molecular-scale simulation
- Field scale problems
- Basic to applied research

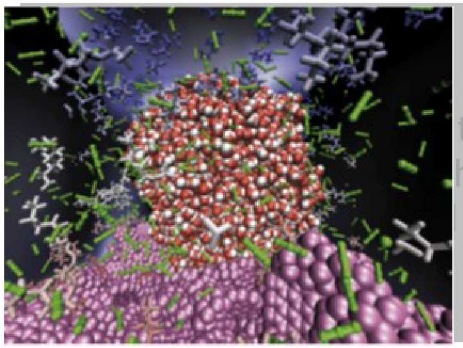

Physical Chemistry Chemical Physics

Enhancement of oil flow in shale nanopores by manipulating friction and viscosity
Tuan A. Ho and Yifeng Wang

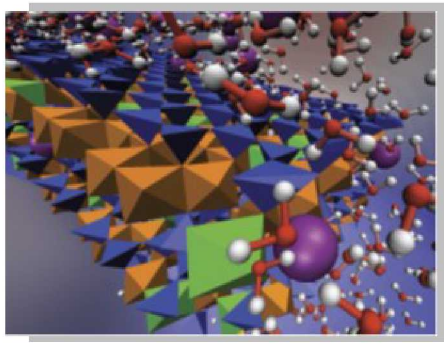

Environmental Science Nano

"Switching on" iron in clay minerals

A. G. Ilgen *et al.*

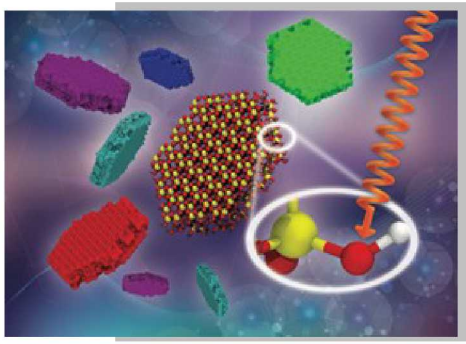

Royal Society of Chemistry Chem. Comm.

Distinguishing Between Bulk and Edge Hydroxyl Vibrational Properties of 2:1 Phyllosilicates via Deuteration
J Harvey *et al.*

# Projects – a sampling

- Geochemistry under nano-scale confinement
- Hydrocarbon/fluid modeling, $CO_2$, $CH_4$; applications to upstream enhanced oil recovery. Modeling, Machine learning
- Chemically-assisted Fracture
- Stress Intensity Thresholds for Development of Reliable Brittle Materials
- Peridynamics/PFLOTRAN
  - Adsorption and degradation of chemical contaminants.
- Isotopic fractionation as in situ sensor of subsurface reactive flow and precursor for rock failure
- Predicting Gas Transport in the Subsurface
- Partitioning of Complex Fluids at Mineral Surfaces

# Experimental Geochemistry




3,000ft$^2$ of laboratory space

Capabilities - Quantitative chemical analysis and characterization of aqueous and solid samples:

- Instruments: ICP-MS, ICP-OES, TGA, FT-IR, Raman microscope, optical microscopes, UV-vis, SEM, XRD, XRF, TGA, nanoindenter.
- Trace metal analysis in liquids;
- Quantitative chemical analysis of solids;
- Spectroscopic characterization and phase ID in solids;
- Microscale elemental and phase mapping of heterogeneous solids;
- Aqueous speciation analysis;

# Molecular Modeling

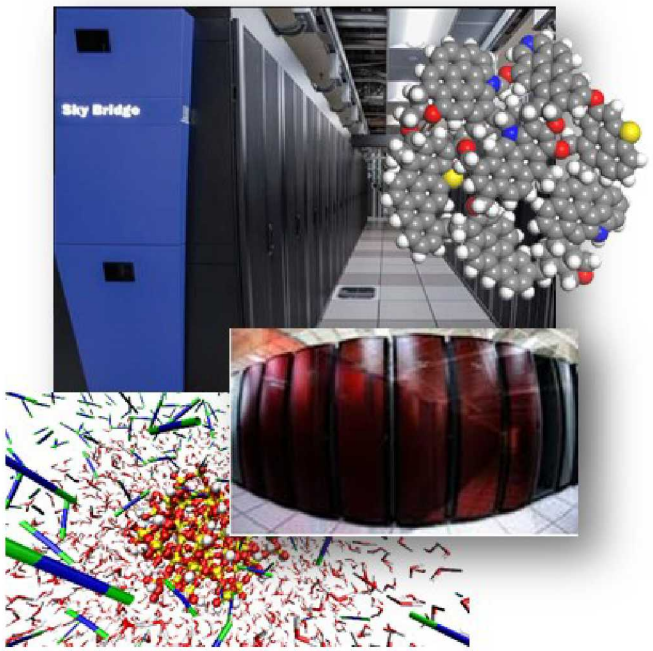


Computing facilities for molecular modeling include a cluster maintained by the Geochemistry Department as well as the Sandia High Performance Computing facilities.

## Molecular Geochemistry

Atomistic simulation with applications to geochemistry, materials science, and related areas.

- Molecular dynamics (classical and ab initio)
- Grand canonical Monte Carlo
- Quantum chemistry (density functional theory)
- Adsorption and surface complexation modeling
- Upscaling from atomistic to continuum-scale models
- Aqueous speciation, solubility and reactive transport modeling
- Ion-ion and ion-surface potential of mean force calculations
- Validation with spectroscopy (nuclear magnetic resonance, inelastic neutron scattering, infrared/Raman)

# Louise Criscenti - Biography


1. Raised in Needham, MA
2. B.S., Brown University, Providence RI
3. M.S., University of Washington, Seattle, WA
4. Research Scientist, PNNL, Richland, WA
5. Research Scientist, PNNL → EPA, Athens, GA
6. Ph.D. Johns Hopkins University, Baltimore, MD
7. Postdoc, PennState, University Park, PA
8. Sandia National Laboratories
   Postdoc, LTE, SMTS, PMTS

# Shale Gas Revolution

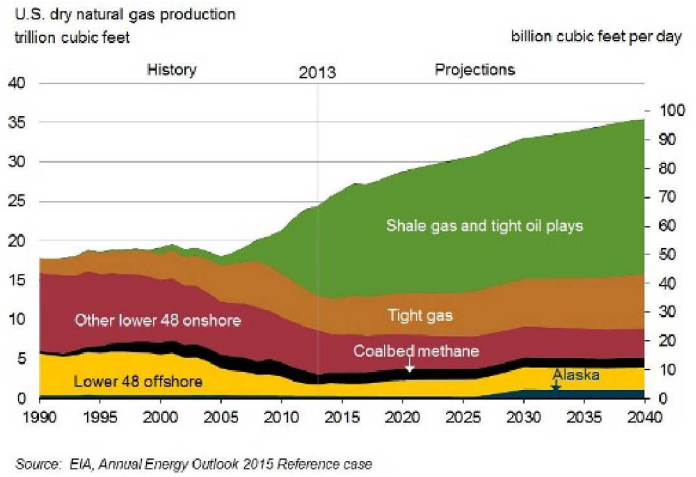


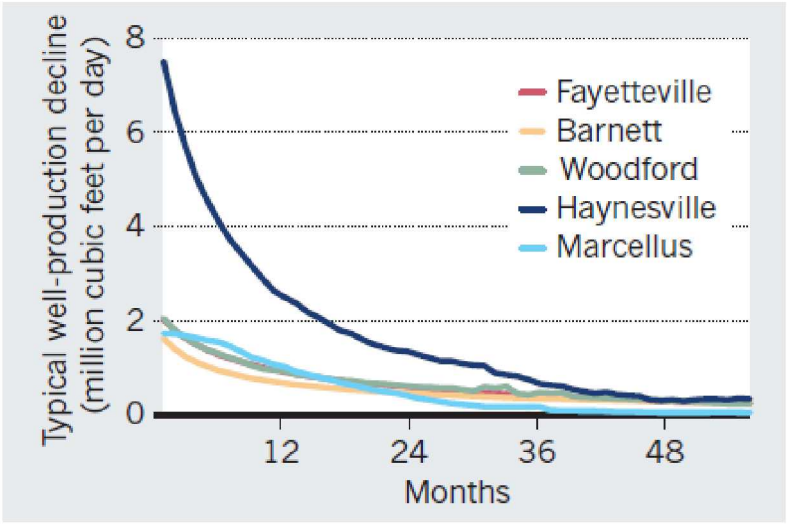


*Hughes, Nature 494, 307 (2013)*

## Major concerns of shale gas:

- Steep decline in productivity over the first 3 years
- Large uncertainty in the long-term projection of decline curves

- A reliable projection of gas production over time must rely on a mechanistic understanding of methane release in shale matrix.
- Molecular simulations are used to study methane disposition and release in kerogen matrix at nanoscale.

# Nanoscale to Macroscale

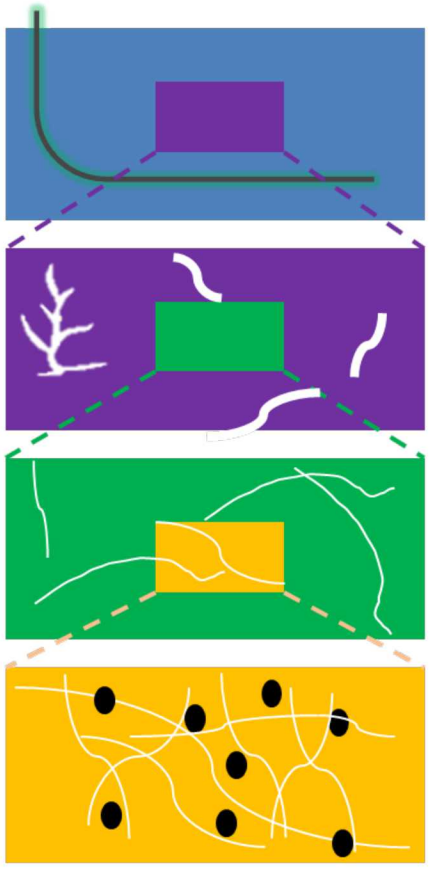

**Macroscale**: gas flow to the wellbore

**Mesoscale**: micro-fractures network

**Microscale**: nanopores network

**Nanoscale/Sub-nanoscale**: Gas diffusion from kerogen/clay porous structure to nanopores.

*JCPT 46, 55 -61 (2007)*

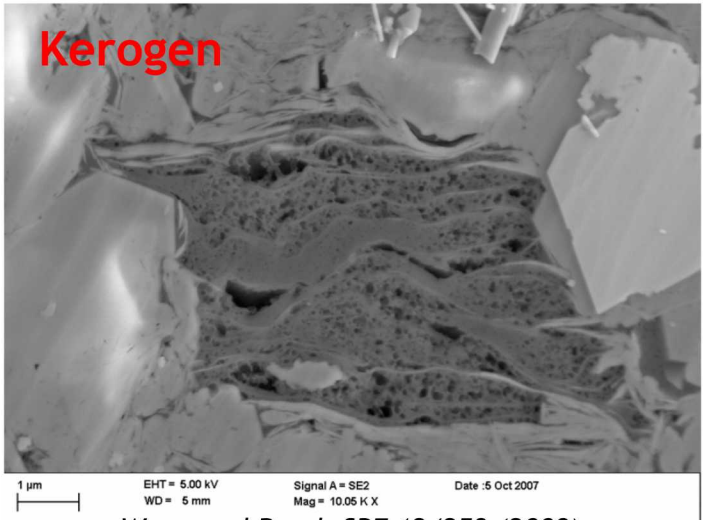


*Wang and Reed, SPE 124253 (2009)*

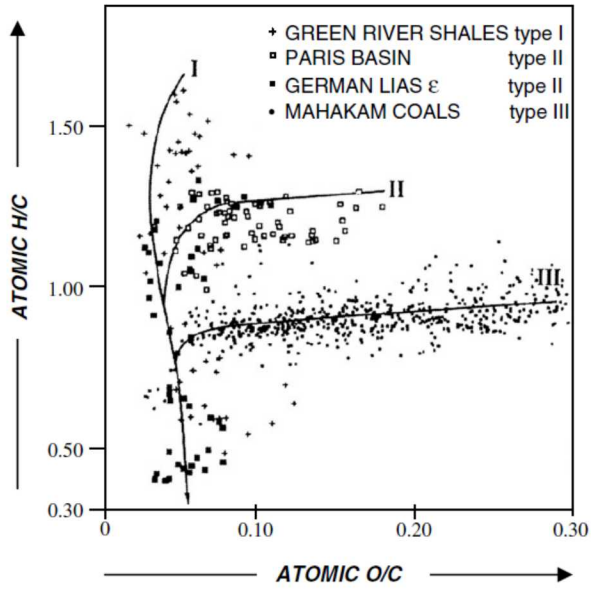


*Vandenbroucke, Org. Geochem. 38, 719-833 (2007)*

# Kerogen Type II Maturation

## Van Krevelen diagram

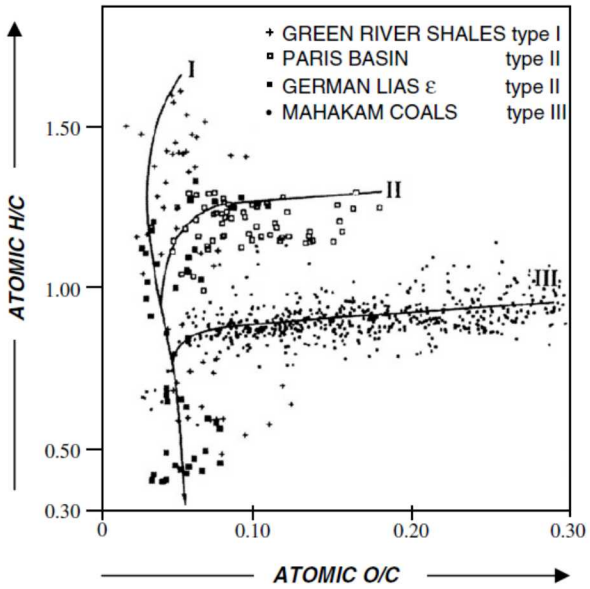


*Vandenbroucke, Org. Geochem. 38, 719-833 (2007)*

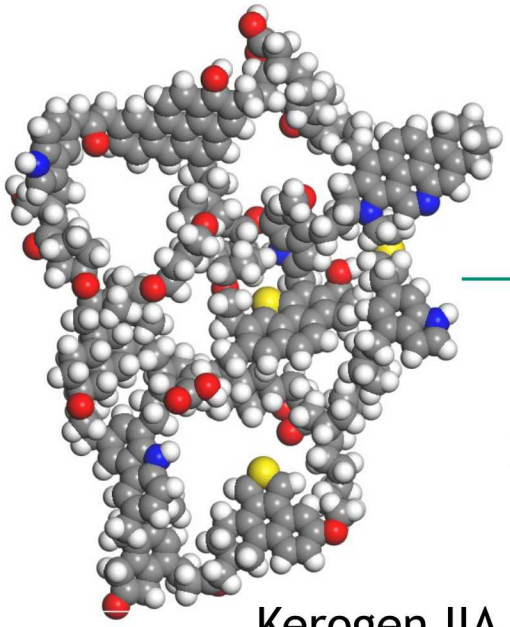

Kerogen IIA

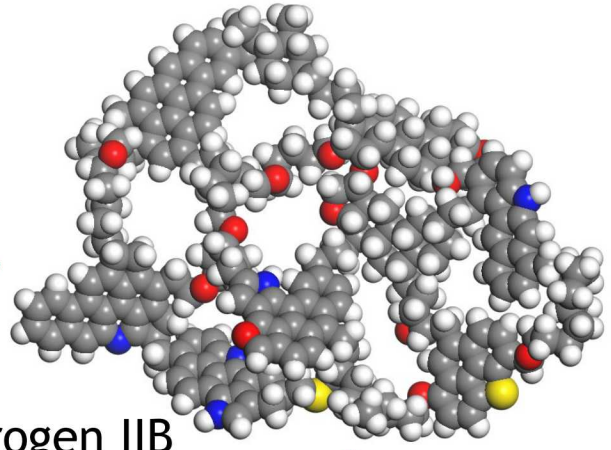

Kerogen IIB

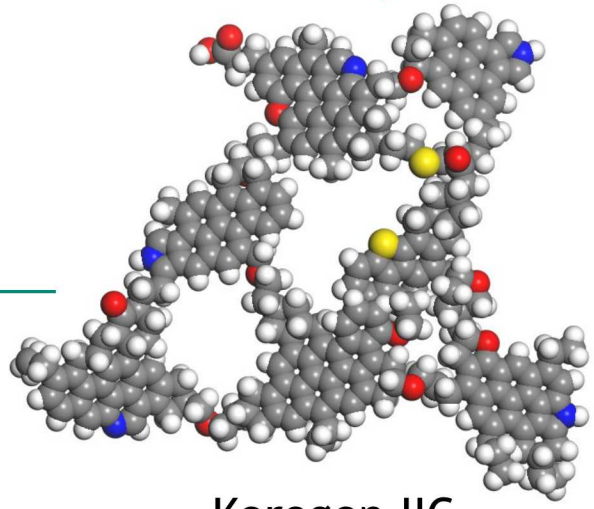

Kerogen IIC

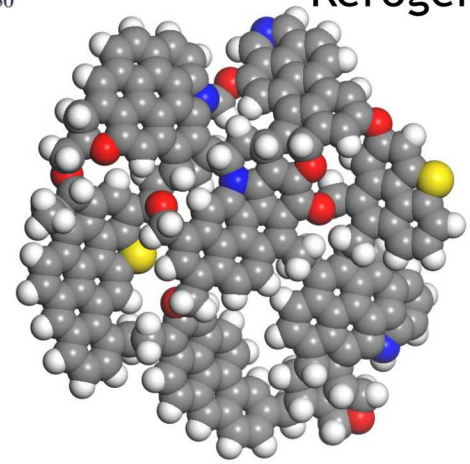

Kerogen IID

> Maturation
> Aromaticity
< Functional Groups

O
N
S
H
C

*Ungerer et al., Energy & Fuel 29, 91-105*

# Formation of Condensed Kerogen

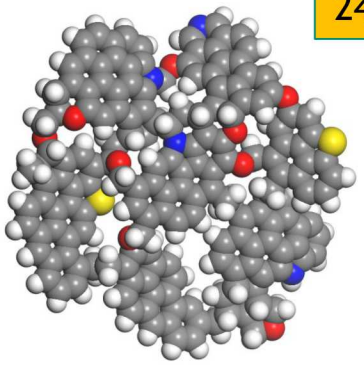

$C_{175}H_{102}O_9N_4S_2$

*Ungerer et al. 2015*
*Energy Fuels 29, 91-105*

24 Kerogens in 10x10x10nm$^3$ box, 1000K

NVT

9 snapshots

NPT, 100atm 900K to 300K

300K and 100atm

NPT, 1atm, *300K*

9 samples at 300K and 1atm

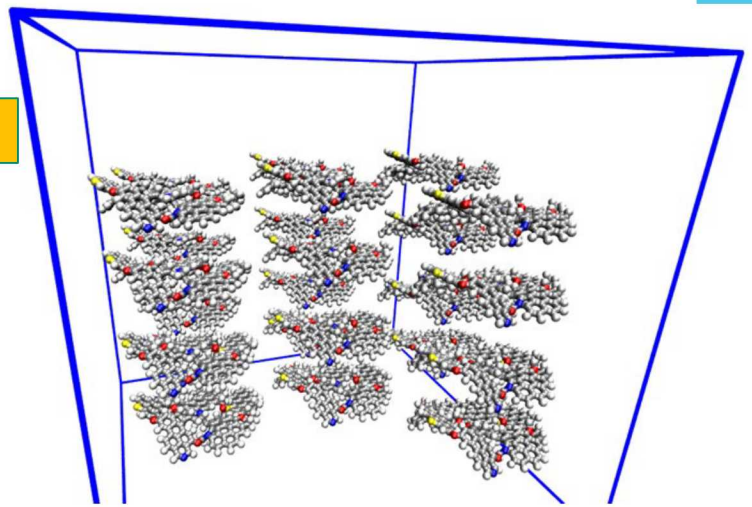

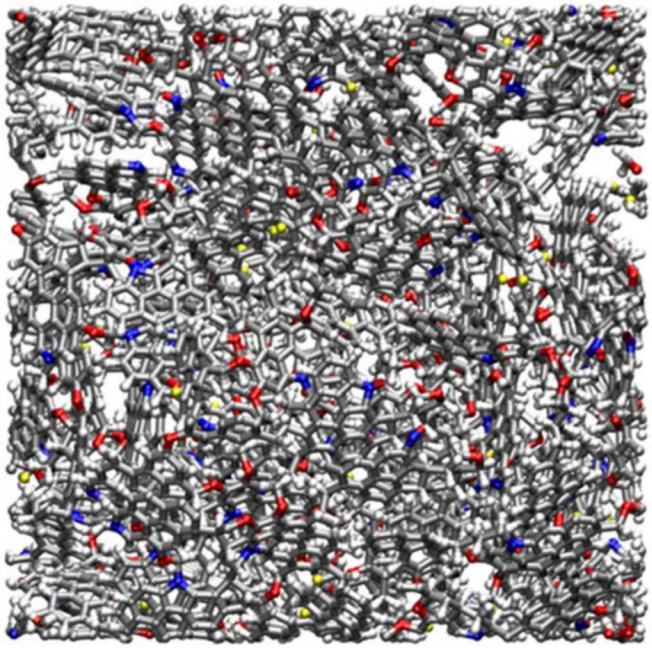

# Characterization

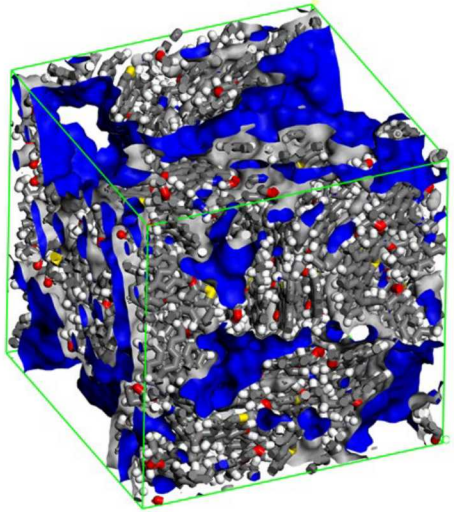

## Density

**Sample 1: 1.172g/cm$^3$**

**Sample 2: 1.287g/cm$^3$**

**Average: 1.22±0.04 g/cm$^3$**

**Experiment: 1.28±0.3g/cm$^3$**

Stankiewicz A, *et al.* (2015) Kerogen density revisited – lessons from the Duvernay Shale. *In: Paper URTeC 2157904 at the Unconventional Resources Technology Conference, San Antonio, Texas, July 2015*

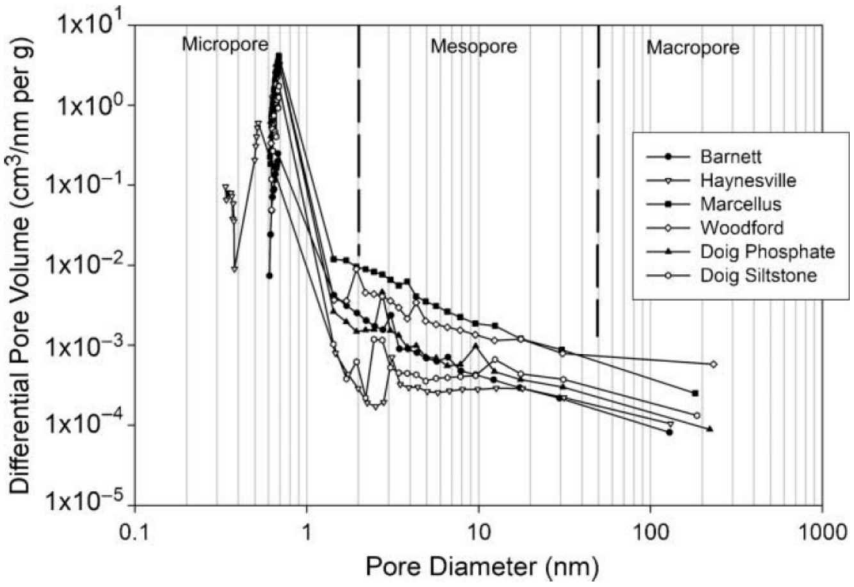


*Chalmers et al. (2012) AAPG 96, 1099-1119*

## Pore size distribution

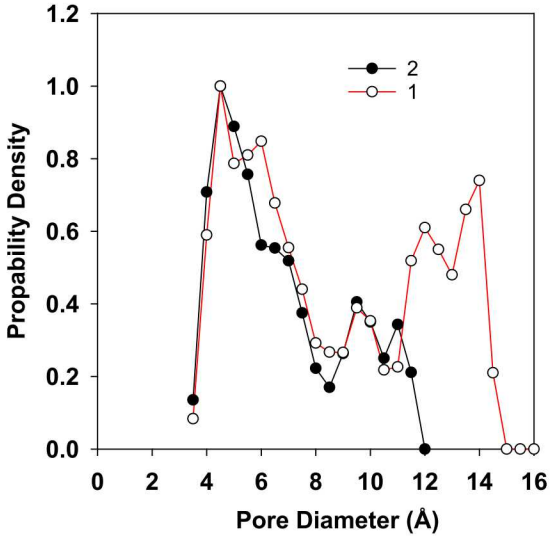


**Method:** Bhattacharya S & Gubbins KE (2006) *Langmuir* 22:7726-7731

# Methane adsorption

## Method: GCMC (μVT)

- Gas in kerogen is in equilibrium with gas in an imaginary reservoir
- Performed "empty box" simulations to establish gas pressures at specific chemical potentials.
- Methane – United atom TRaPPE FF
- T = 338K

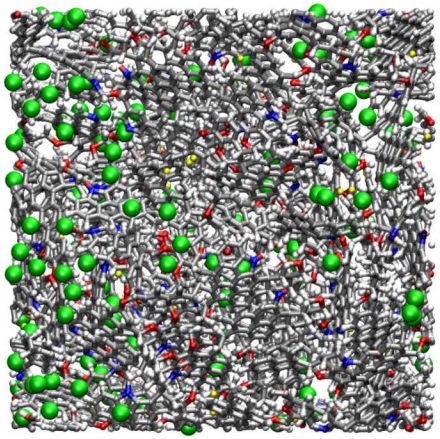

Methane

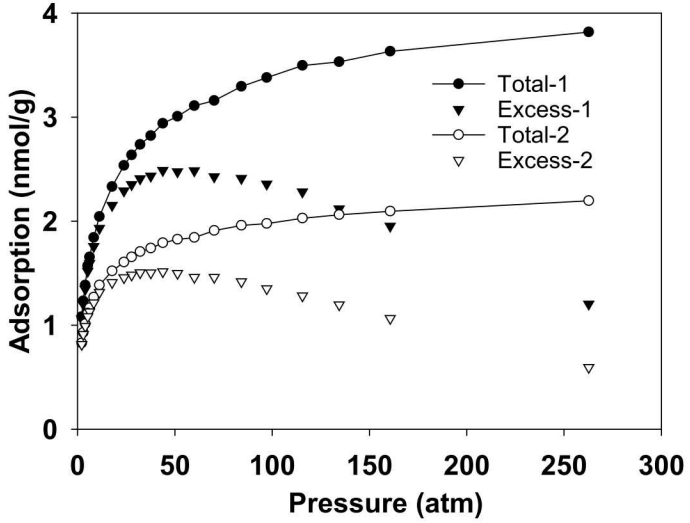


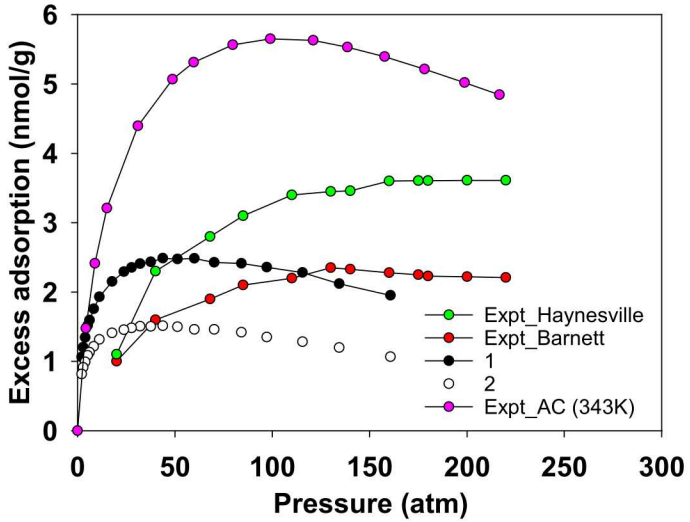


$$n_{excess} = n_{total} - \rho_{P,T} V_{free}$$

| Excess Adsorption | Total Adsorption | Gas Density | Pore Volume |
|---|---|---|---|

*Gasparik et al. (2014) Int J Coal Geol* **123**, 34-51.
*Herbst and Harting (2002) Adsorption* **8**, *111-123.*

# Methane extraction from kerogen

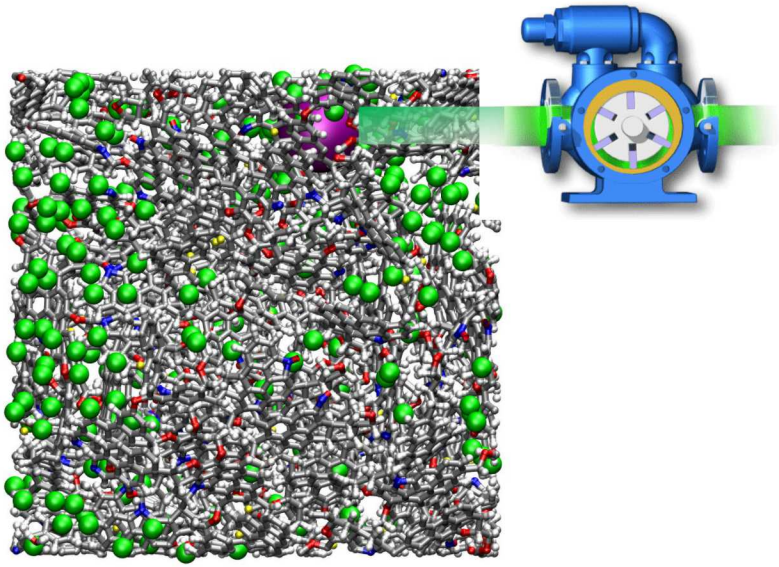

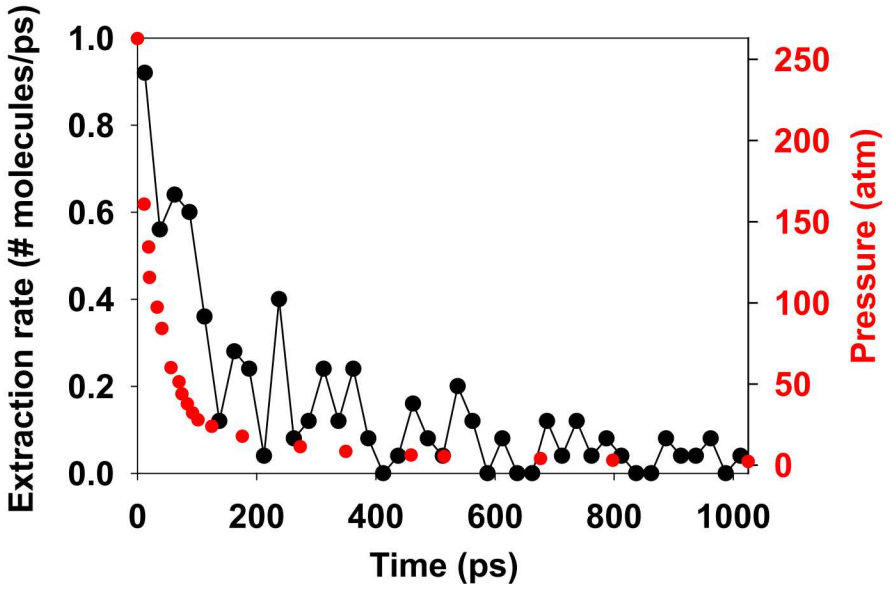


- Two stages of gas release
- Pore network connectivity can significantly affect the ultimate recovery

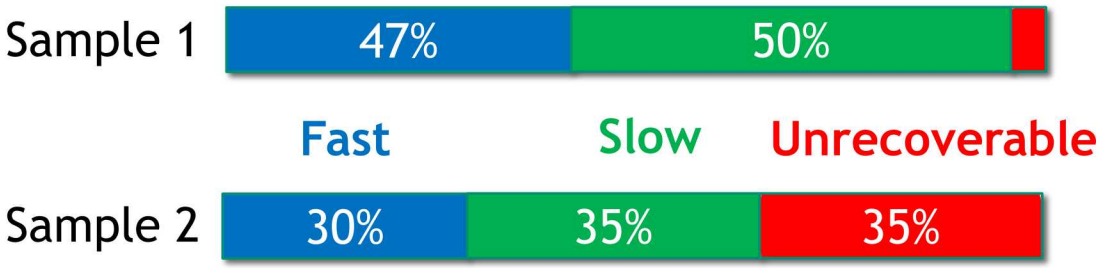


*Ho et al. (2016) Nature Scientific Reports, DOI: 10.1038/srep28053*

# Methane and Carbon Dioxide Adsorption

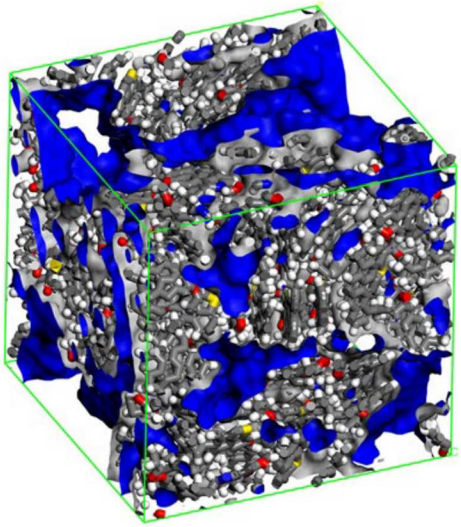

- Both carbon dioxide and methane are generated during kerogen maturation.
- Grand Canonical Monte Carlo molecular simulations (TOWHEE)
  - Scenario 1: Pure CH4 or Pure CO2
  - Scenario 2: 1:1 Binary Mixture
- Kerogen preferentially retains $CO_2$ over $CH_4$.

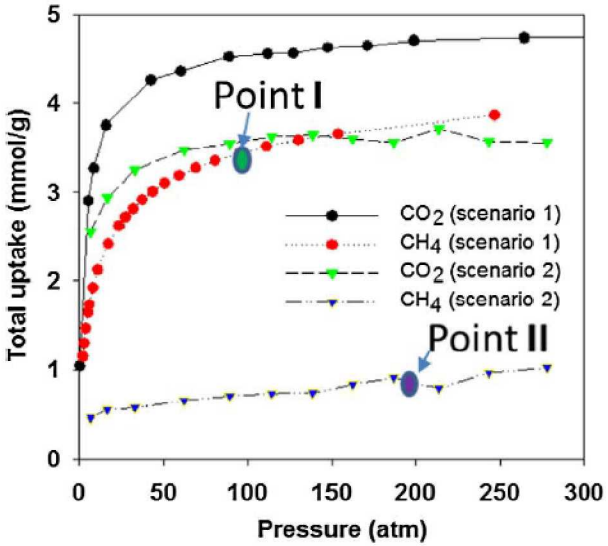


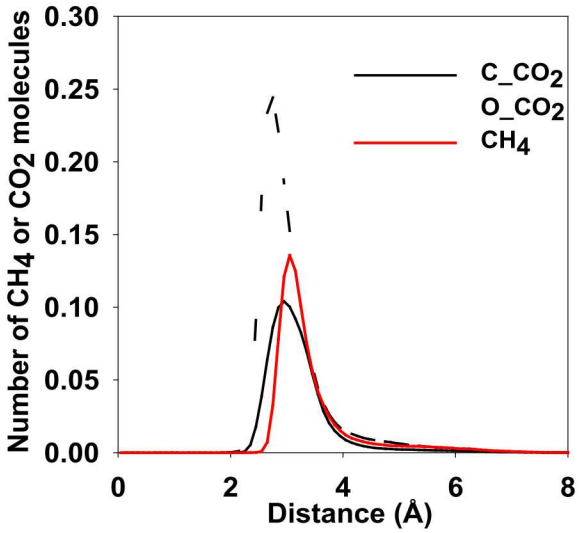


*Ho et al. (2018a) Fuel, 220, 1-7, 2018.*

# Summary

- Methane and carbon dioxide are two major components generated during kerogen maturation.
- For methane alone, there are two stages of methane gas release – first “free gas” is released, then “adsorbed gas” is released.

- Kerogen preferentially retains $CO_2$ over $CH_4$. The majority of $CO_2$ either generated during kerogen maturation or injected in EOR will remain trapped in kerogen.
- Water can block $CH_4$ release. However, $CO_2$ may enhance $CH_4$ release because dissolved $CO_2$ can migrate through water and exchange for adsorbed methane in kerogen nanopores.

- Kerogen volume can expand by 5.4% upon $CH_4$ adsorption and 11% upon $CO_2$ adsorption.
- Volume expansion quadratically increases with increasing gas adsorption, indicating surface layer of adsorbed gas is critical to causing volumetric strain.
- Kerogen swelling may need to be considered in estimates of gas-in-place or gas storage capacity for subsurface carbon sequestration.

# Introduction

- The objective is to use molecular simulation to investigate aqueous ion diffusion and adsorption to mineral surfaces in complex systems that are more representative of compact soils and rocks.
- Gibbsite is used as a model mineral because it has properties similar to a clay mineral but does not include the additional complexity of an interlayer.
- Molecular simulations are performed for:
  - Water and ion adsorption to the basal (001) and edge (100) gibbsite surfaces
  - Water and ion adsorption to a gibbsite nanoparticle
  - Water adsorption to gibbsite nanoparticle aggregates that are created through de-watering and compaction

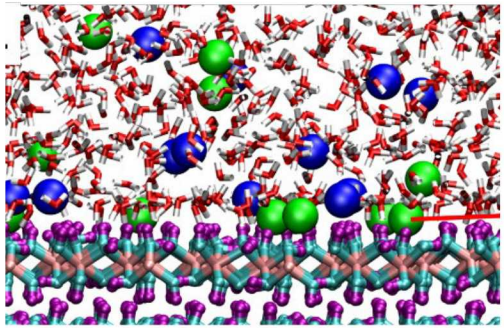

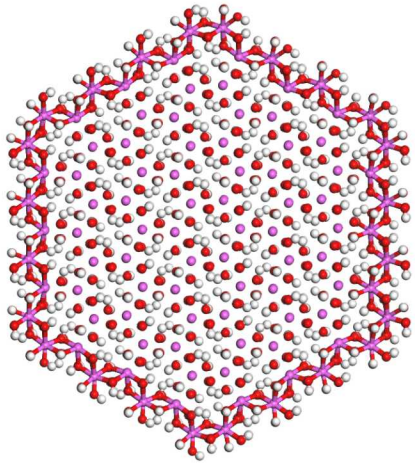

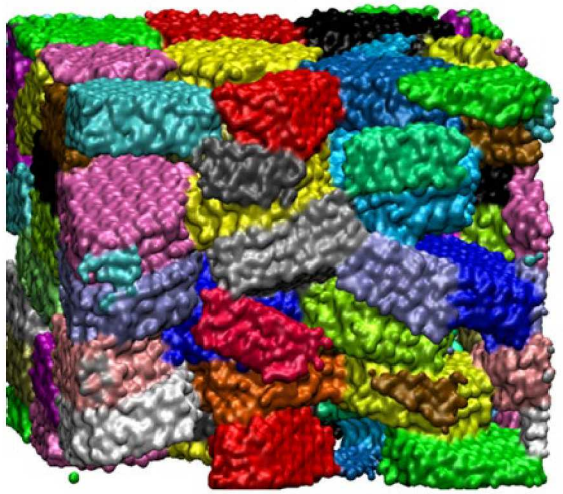

# Adsorption on Gibbsite basal (001) and edge (100) surfaces

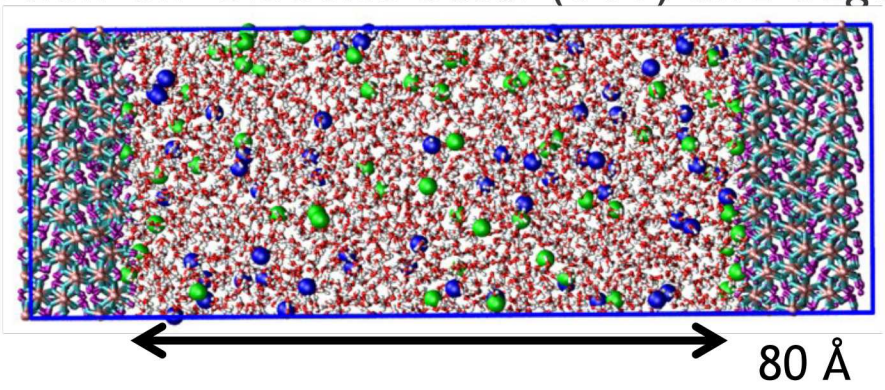


**Molecular dynamics**

- LAMMPS code with ClayFF force field.
- New Al-O-H angle bending term for stability of edge sites (Pouvreau et al., 2017)

Al
O
H
$O_w$
$H_w$
Na
Cl

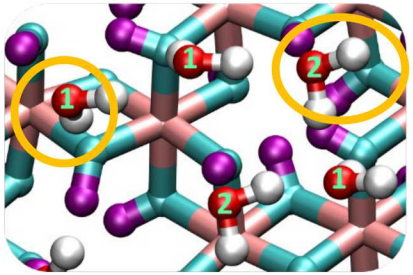


(001)

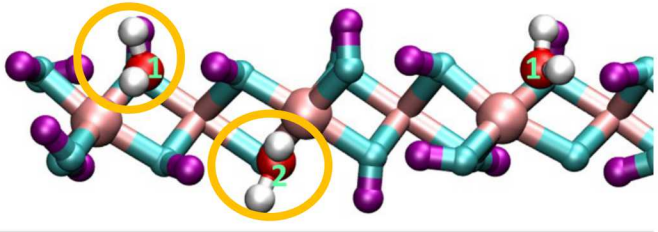


(100)

Water adsorption sites

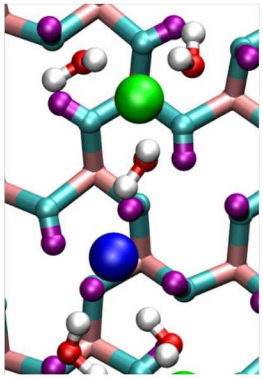

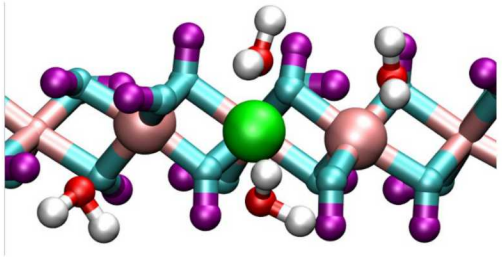

Ion adsorption sites

Ho, T.A., Greathouse, J.A., Lee, A.S. and Criscenti, L.J. (2018) Enhanced Ion Adsorption on Mineral Nanoparticles. Langmuir 34, 5926-5934.

# Cation Adsorption to Gibbsite Surfaces

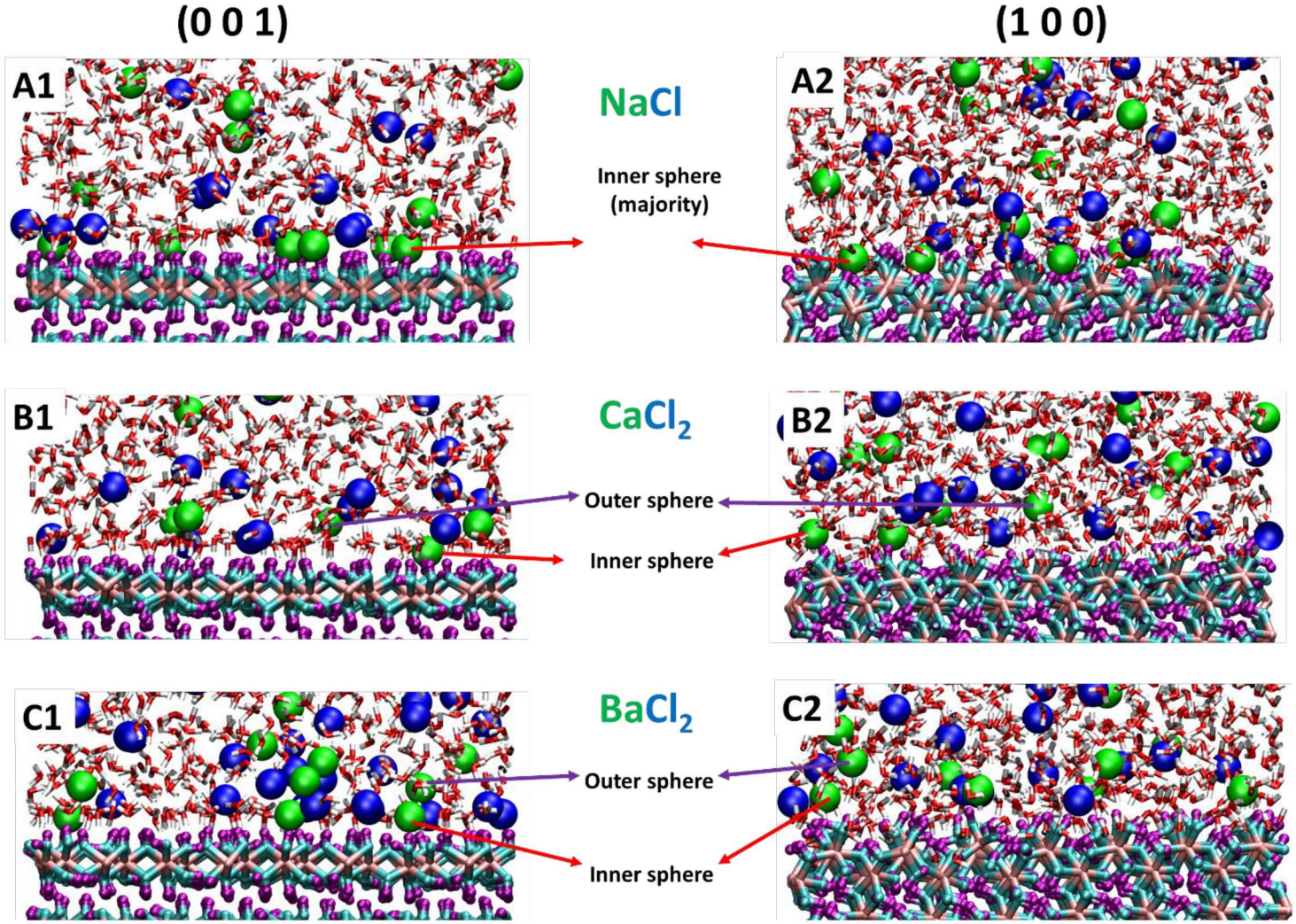


Ho, T.A., Greathouse, J.A., Lee, A.S. and Criscenti, L.J. (2018) Enhanced Ion Adsorption on Mineral Nanoparticles. Langmuir 34, 5926-5934.

# Gibbsite nanoparticle construction

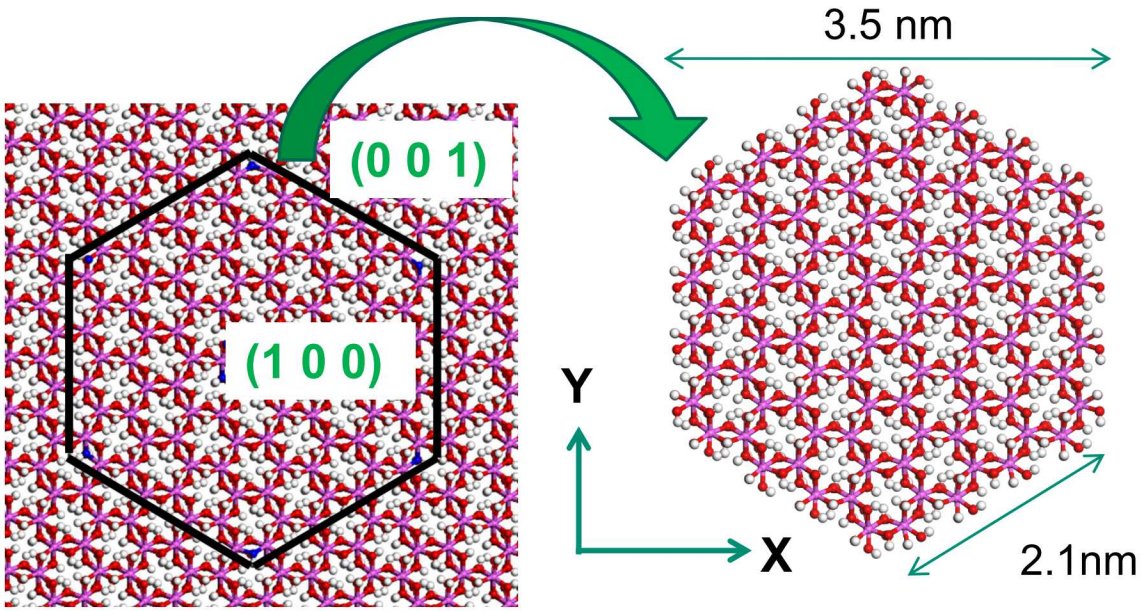


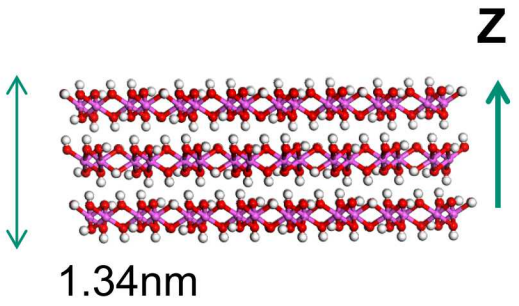


Lateral dimension 2.1 – 3.5 nm
Particle thickness 3 layers (1.3 nm)

Exploit the hexagonal symmetry of bulk gibbsite

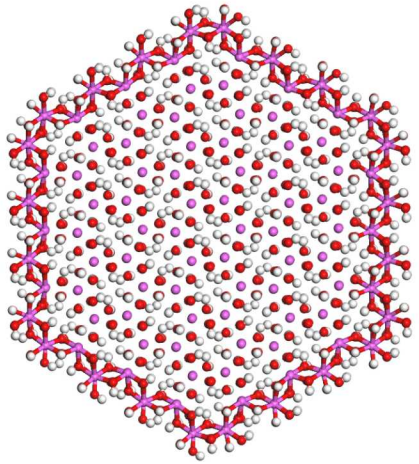

**Molecular dynamics**

- LAMMPS code with ClayFF parameters.
- New Al-O-H angle bending term for stability of edge sites.
- Extra Al-O-Al term added for nanoparticle stability.

# Comparison of Adsorption on Gibbsite Nanoparticle vs. Surfaces

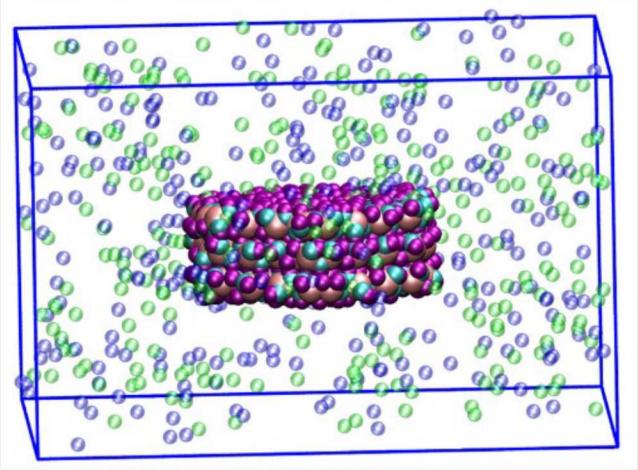

- $Cl^-$ adsorption is not enhanced on NP
- $Na^+$, $Ca^{2+}$, and $Ba^{2+}$ adsorption are enhanced on NP
- NPs exhibit higher concentrations of IS complexes

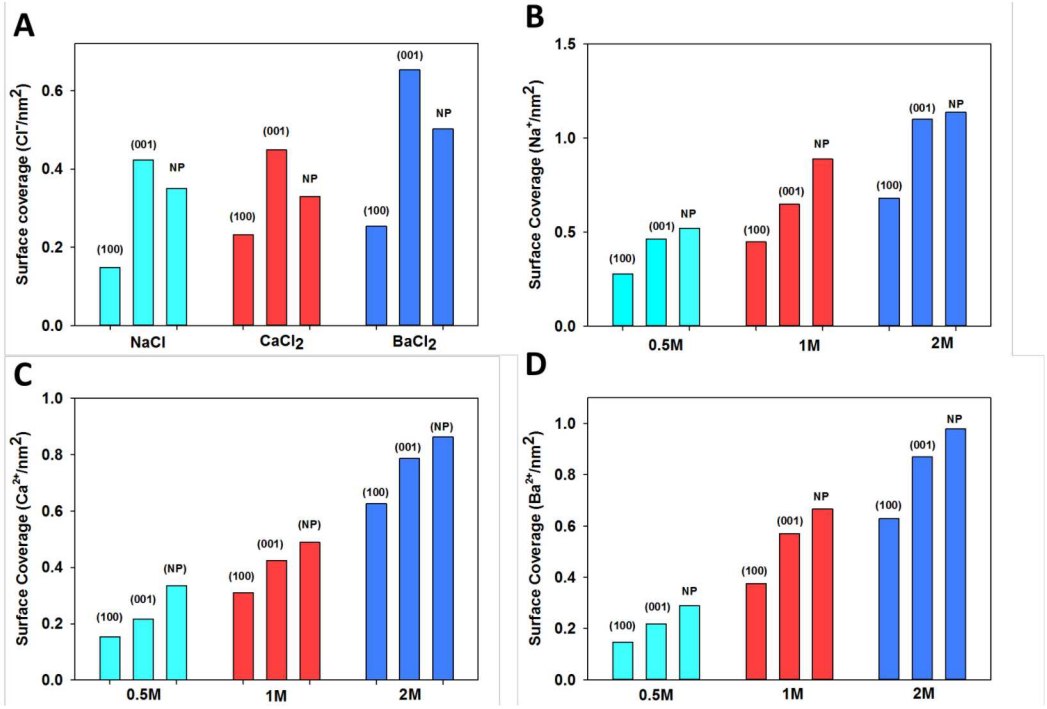


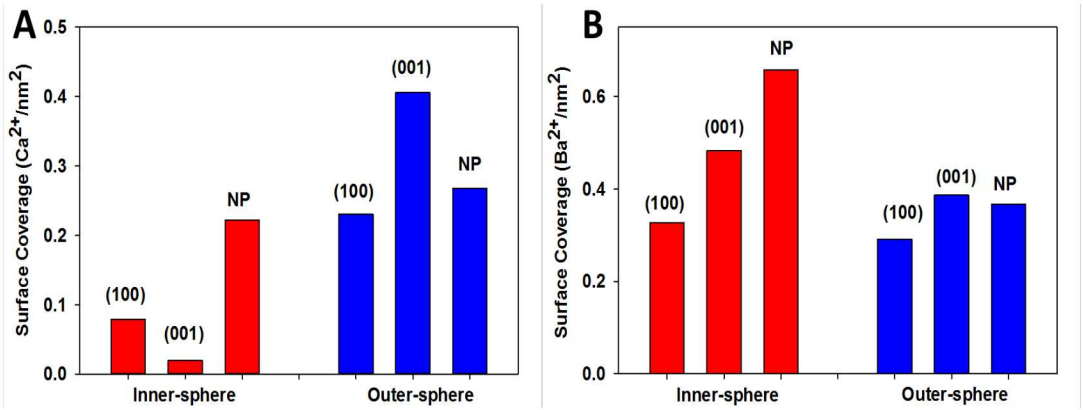


Ho, T.A., Greathouse, J.A., Lee, A.S. and Criscenti, L.J. (2018) Enhanced Ion Adsorption on Mineral Nanoparticles. Langmuir 34, 5926-5934.

# Cation Adsorption at Nanoparticle Corners

Snap-shots

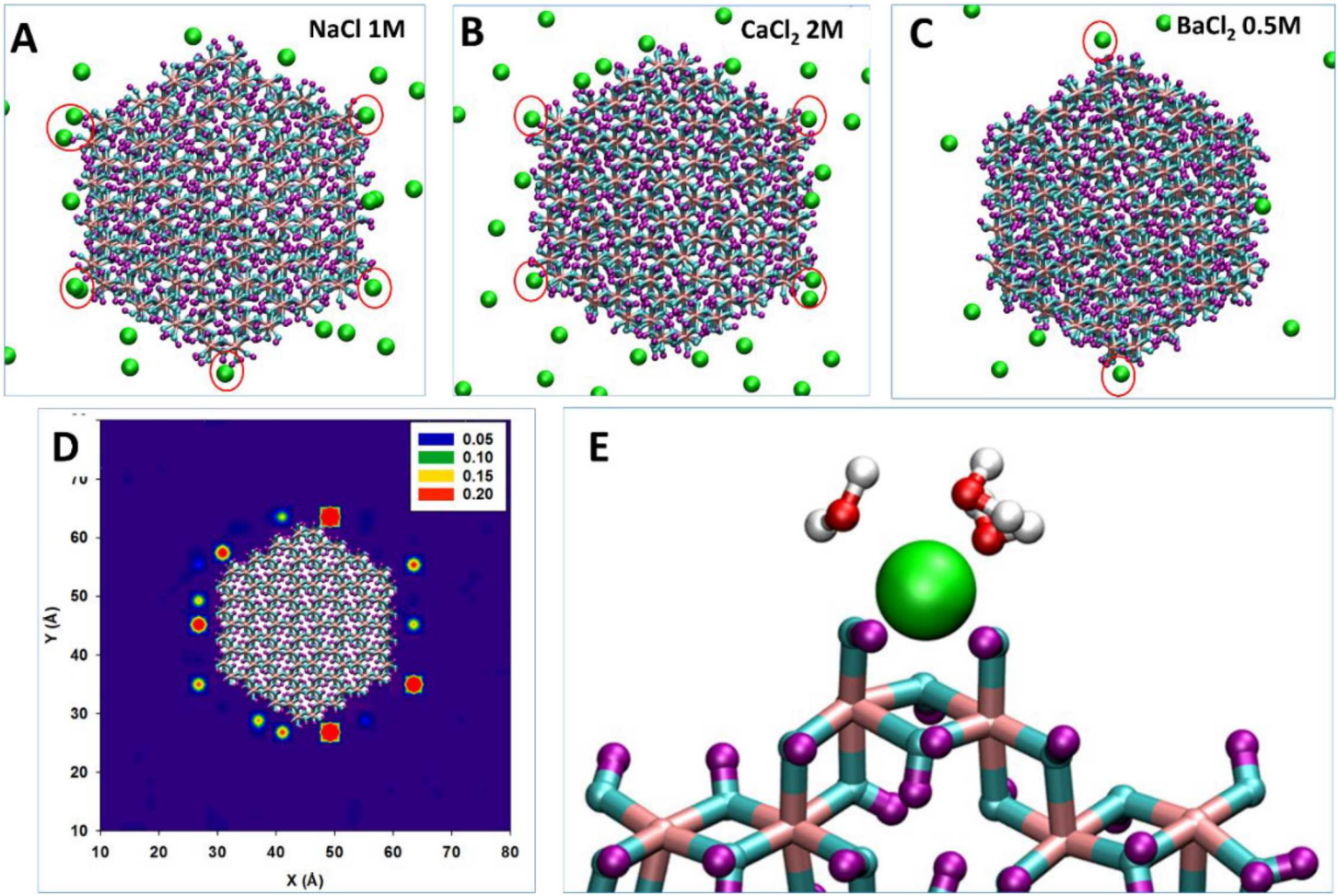


Planar density distribution
$Na^+$ over 10 ns

Ho, T.A., Greathouse, J.A., Lee, A.S. and Criscenti, L.J. (2018) Enhanced Ion Adsorption on Mineral Nanoparticles. Langmuir 34, 5926-5934.

# Gibbsite aggregation

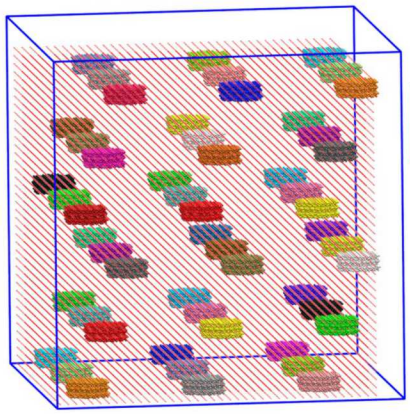

54 NPs, 55k $H_2O$
30 x 30 x 30 $nm^3$

NVT
0.3 ns
300 K

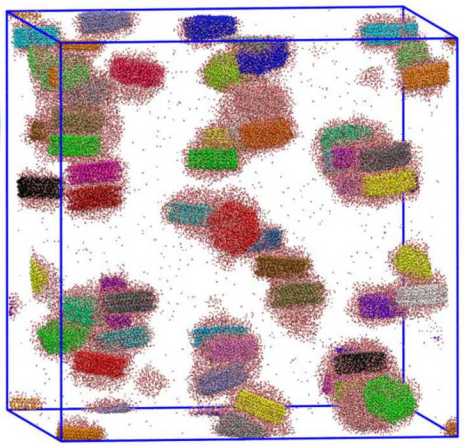

NPT
0.3 ns
300 K
100 MPa

Hydrated aggregate
15 x 15 x 15 $nm^3$

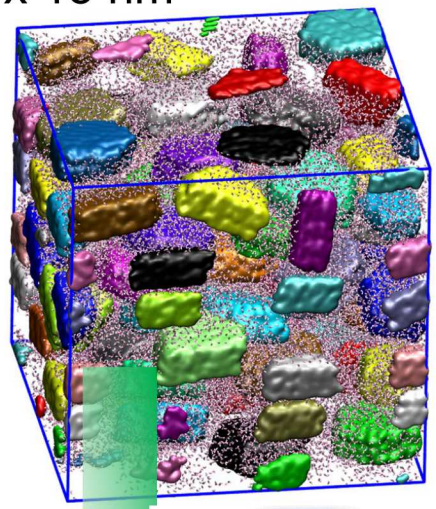

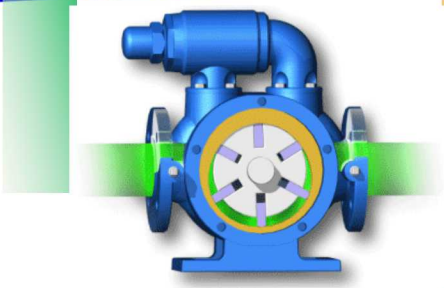

**Effect of dewatering rate:**

- Delete all water: "Fast"
- Delete 100 H2O/100 steps: "Intermediate"
- Delete 10 H2O/100 steps: "Slow"

'Virtual' pump removes waters from a pre-defined region.

**Effect of water content:**

- 1 water layer around each particle: 1W (22.5 wt%)
- 2 water layers around each particle: 2W (37.2 wt%)
- Additional withdraw water from 2W: 2W_dewatering (6 wt%)
- Dry: 2W_dry

Ho, T.A., Greathouse, J.A., Wang, Y. and Criscenti, L.J. (2017) Atomistic structure of mineral nano-aggregates from simulated compaction and dewatering. Scientific Reports 7:15286

# Stacking of nanoparticles

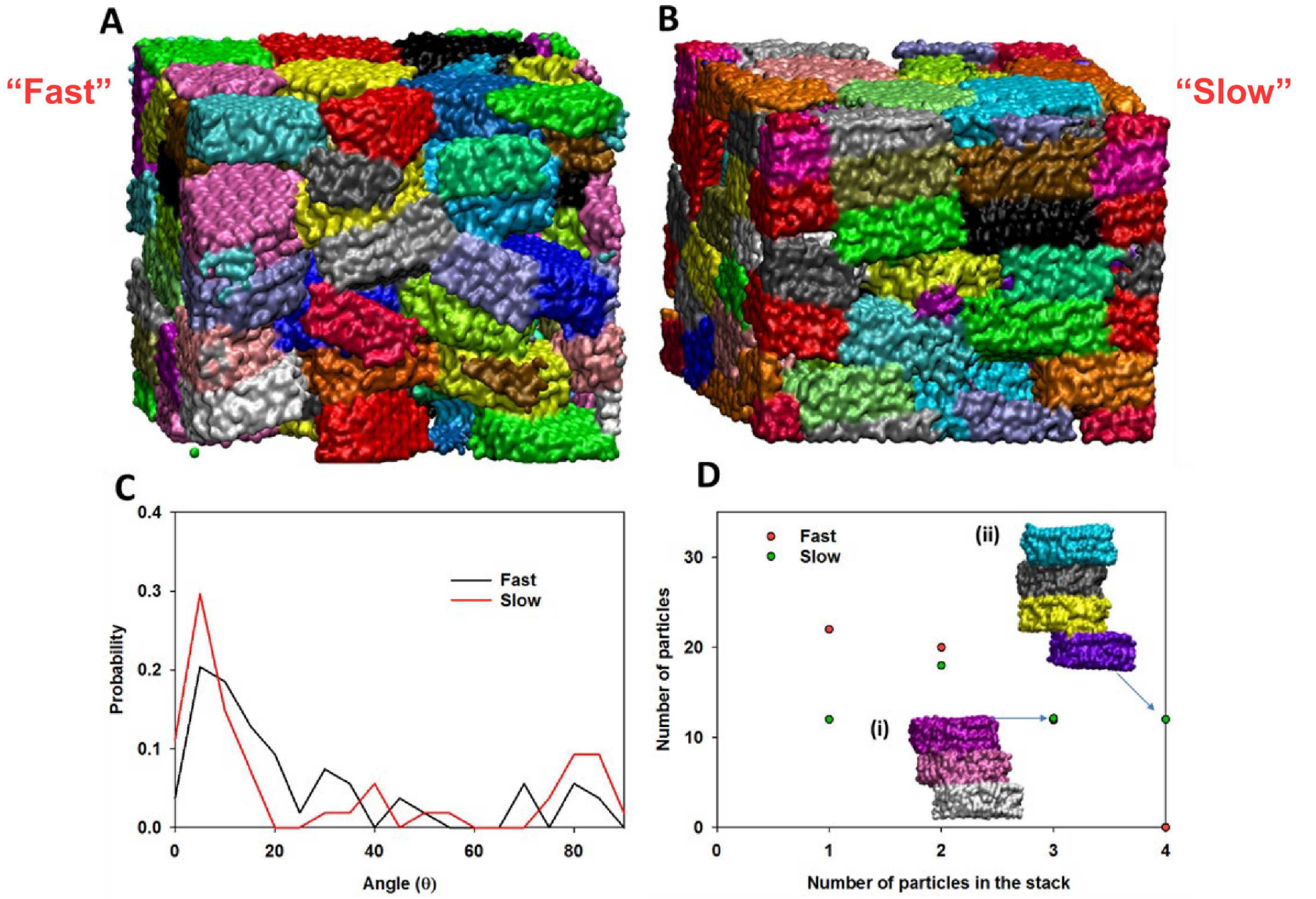


Ho et al.. Scientific Reports 7:15286

# Pore properties

## Effect of dewatering on PSD

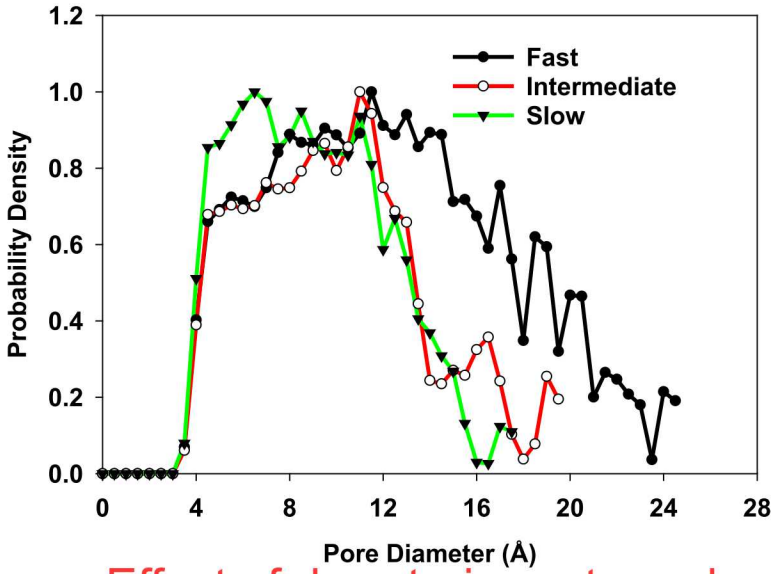


## Effect of water content on PSD

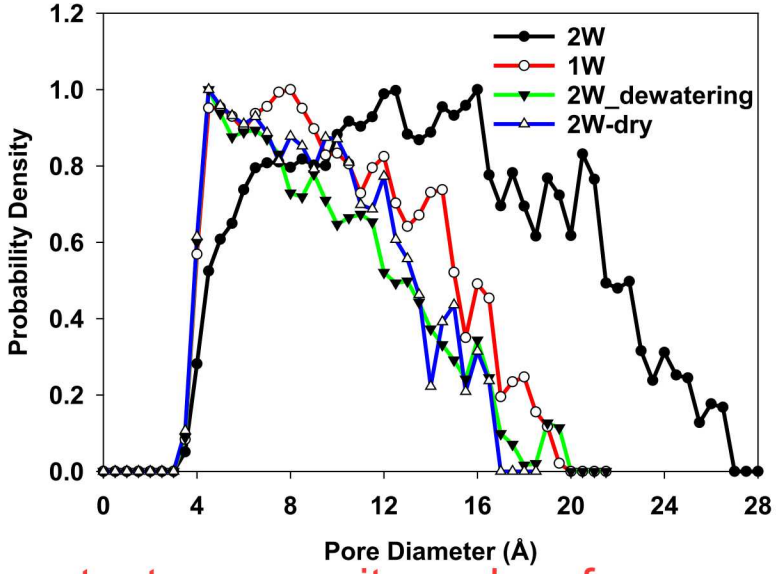


## Effect of dewatering rate and water content on porosity and surface area

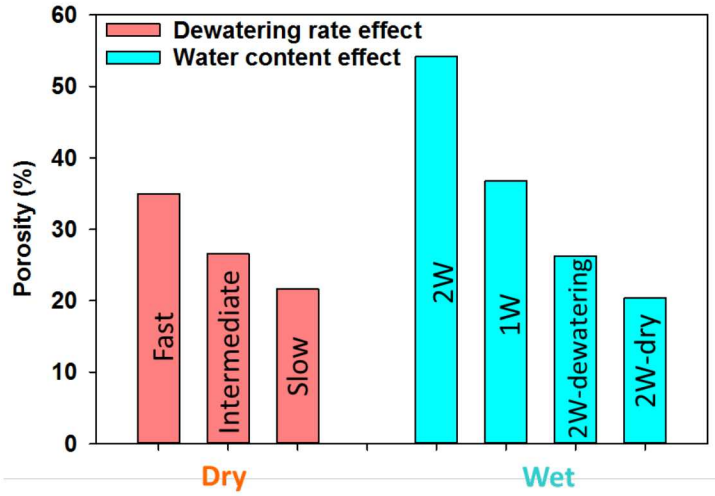


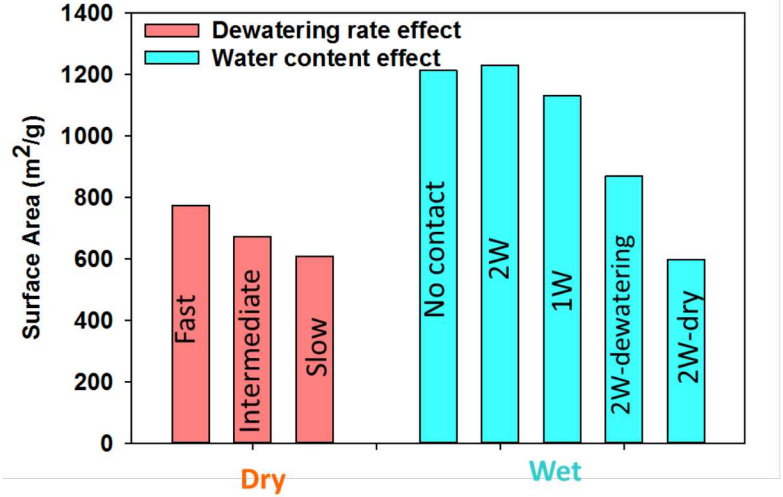


Ho et al.(2017) Scientific Reports 7:15286

# Water structure: 1D atomic density profiles

## 2W water content (37 wt%)

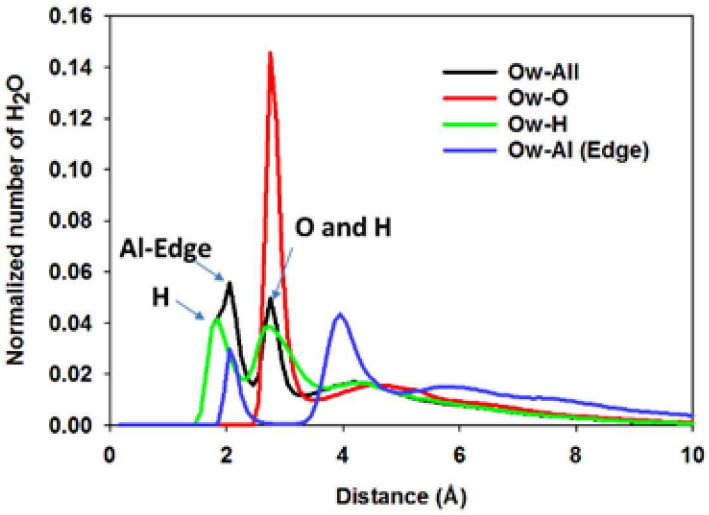


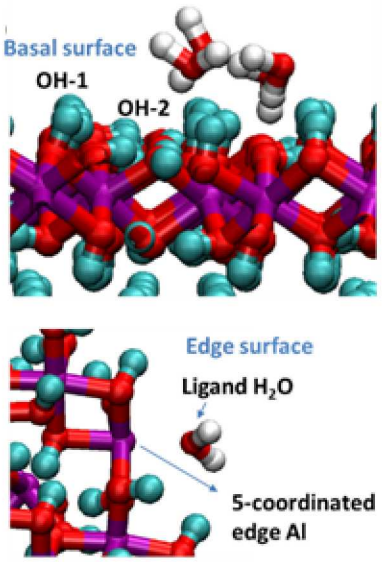


## 1W water content (22 wt%)

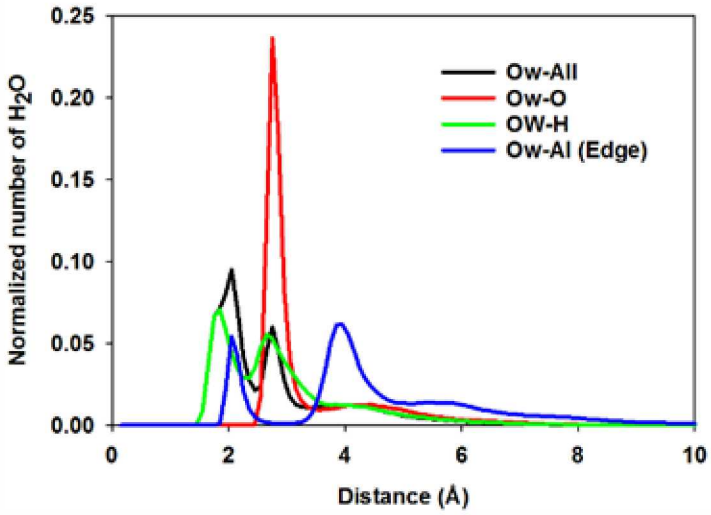


Distinct peaks due to water at basal vs edge surfaces.

Water structure at nanoparticle surfaces qualitatively the same regardless of water content.

- < 5 Å from surface: similar water coordination environments.
- > 5 Å from surface: pore water seen up to 10 Å from surface.

Ho, T.A., Greathouse, J.A., Wang, Y. and Criscenti, L.J. (2017) Atomistic structure of mineral nano-aggregates from simulated compaction and dewatering. Scientific Reports 7:15286

# What's next?

Flow/Diffusion through Columns?

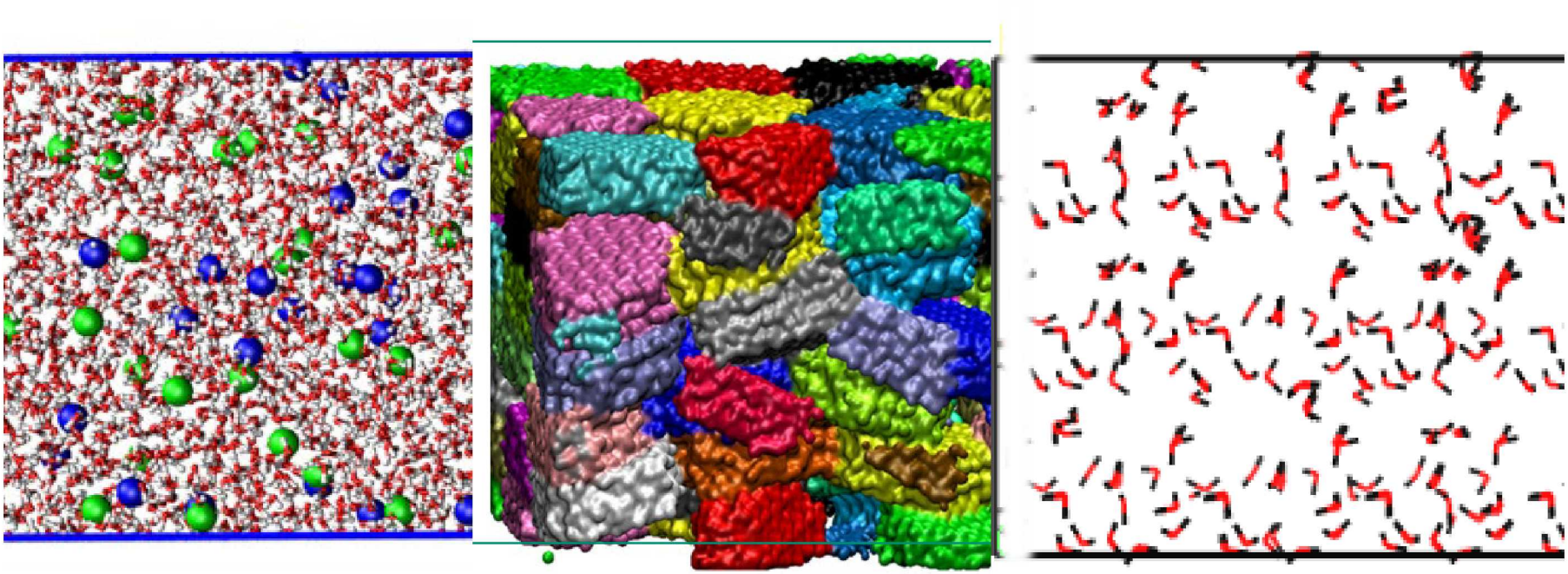

Breakthrough Curves?

# Conclusions

- The percent cation adsorption as inner-sphere complexes depends on the gibbsite surface.
- For all cations, surface coverages are higher on the basal surface than the edge surface.
- For all cations, surface coverages are highest for the nanoparticle, due to the significant number of inner-sphere cations found at nanoparticle corners.
- For the nanoparticle aggregates, slow dewatering creates more compact aggregates that fast dewatering.
- For the aggregates, the amount of water present strongly affects the particle-particle interactions and the aggregate structure.

Work supported by
U.S. DOE BES Geosciences Program
U.S. DOE National Energy Technology Laboratory (NETL)

# Geochemical Reactions in Subcritical Fracture

Subcritical fracture is an example of a nano-confined space – a location where the chemistry of reactions will be impacted by:

- Proximity of two surfaces
- Changes in water structure
- Changes in ion adsorption mechanisms

Fracture geometries are wedge-shaped, introducing the effects of nanoconfinement on geochemical fluids over a range of pore sizes from the tip to the bulk solution.

The chemical reactions that occur in a subcritical fracture impact the mechanical properties of the material and influence fracture propagation.

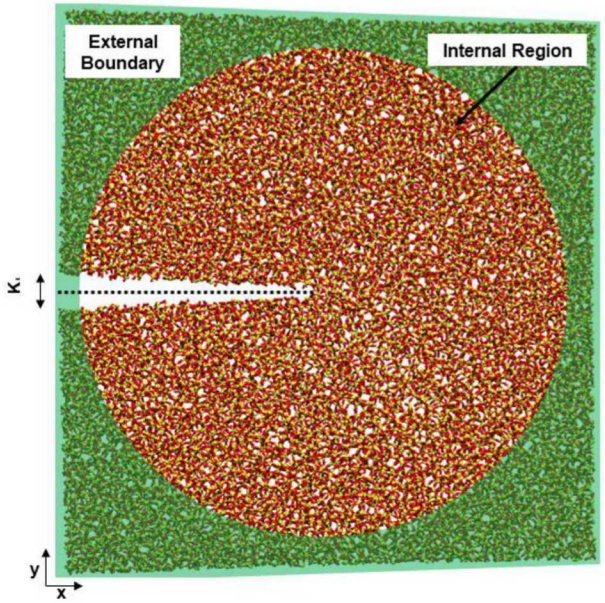


- Schematic of the quasi-2D silica system with a slit crack.
- Bonds are severed to form a slit crack.
- Atoms in the boundary region are fixed to the displacement proscribed by mode I loading
- Radius of cylinder = 3.2 nm
- In the cylindrical region, the atoms are free to relax to a minimum energy configuration
- The axis of the cylinder is out-of-plane and the thickness of the system is 2.8 nm.

# Project Objectives

- Develop a fundamental, atomistic-level understanding of the *chemical-mechanical* processes that **control subcritical cracks** in low-permeability geomaterials.
- Link atomic-scale insight to macroscale observables.
- Address how **chemical environment** affects **mechanical behavior**.

Definitions:

- Classical fracture mechanics: the fracture toughness, $K_{IC}$ is the point at which a pre-existing fracture converts from subcritical to critical behavior.
- Our definition($eK_{IC}$): the loading at which the first fracture event occurs.
- Our $eK_{IC}$ is impacted by the chemical environment unlike the strict $K_{IC}$ which is defined as an intrinsic material property.

# Computational Methods

- Classical molecular dynamics for large scale simulation of silica fracture
- ReaxFF: Bond-order based forcefield including reactive water and silica bond breakage and formation (Fogarty et al. *J. Chem. Phys.* (2010), Yeon and van Duin, *J. Phys. Chem. C.* (2015)

$$E_{Total} = E_{Bond} + E_{Over} + E_{Under} + E_{LP} + E_{Val} + E_{Pen} + E_{Tors} + E_{Conj} + E_{VDW} + E_{Coul}$$

- 2D silica structures (12-replicates) were used.
- Investigated 3 different conditions to isolate chemical and mechanical effects on fracture
- Protocol: Apply initial loading (0.15 MPa$\sqrt{m}$) and relax fracture tip
  - Mechanical: increase loading (stepwise), relax for 5ps at 300K, repeat
  - Chemical-Mechanical: increase loading, add in water, relax for 5ps at 300K, repeat
  - Chemical: maintain loading, relax for 5ps at 300K, repeat

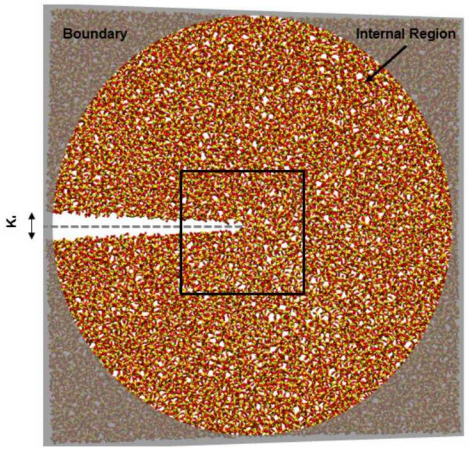


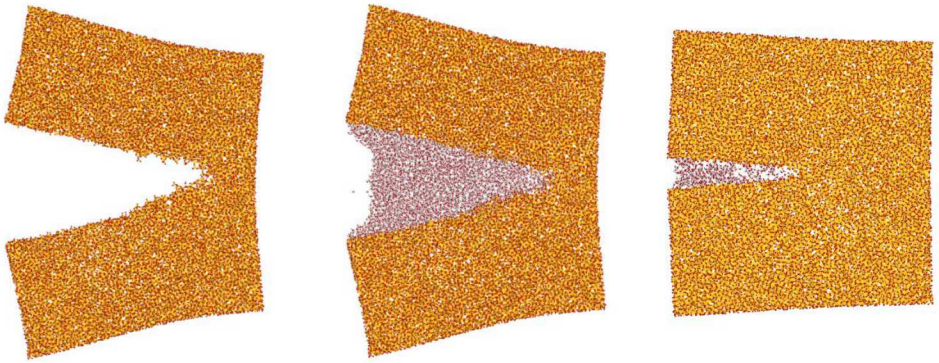

**Mechanical**
(mechanical loading only)

**Chemical-Mechanical**
(aqueous enviorment and mechanical loading)

**Chemical**
(aqueous enviorment only)

# Fracture Toughness in Vacuum and Water

- Identified from variation in the potential energy of the silica during loading
- Earlier fracture of silica in aqueous conditions
- No fracture in chemical-only systems (dissolution)
- $K_{IC}$ is lower than in experimental systems (0.78 MPa√m) due to resolution and temperature effects

Mechanical: 0.339±0.037 MPa√m
Chemical-Mechanical: 0.246±0.074 MPa√M
Reduction in $K_{IC}$: ~26.5%

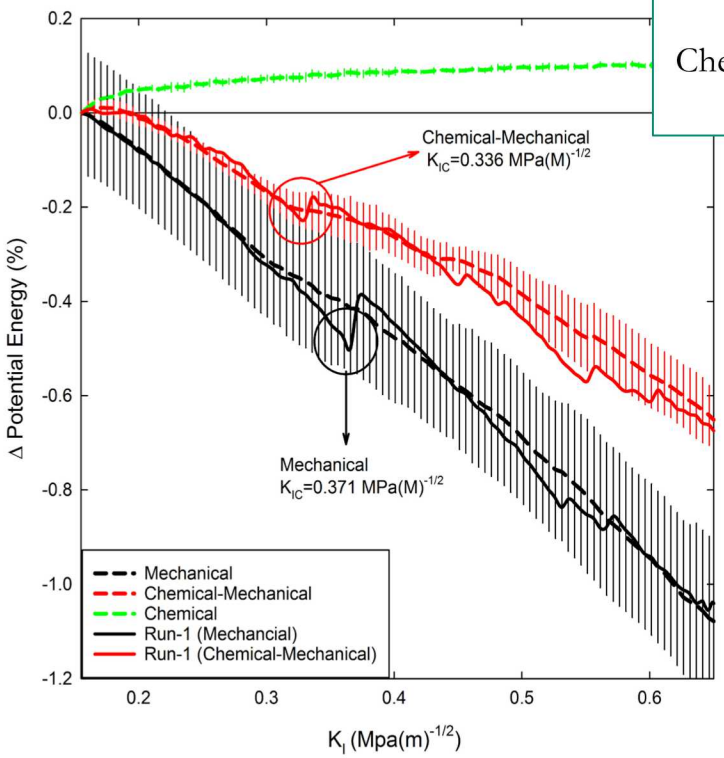


Change in potential energy for silica systems in mechanical, chemical, and chemical-mechanical conditions.

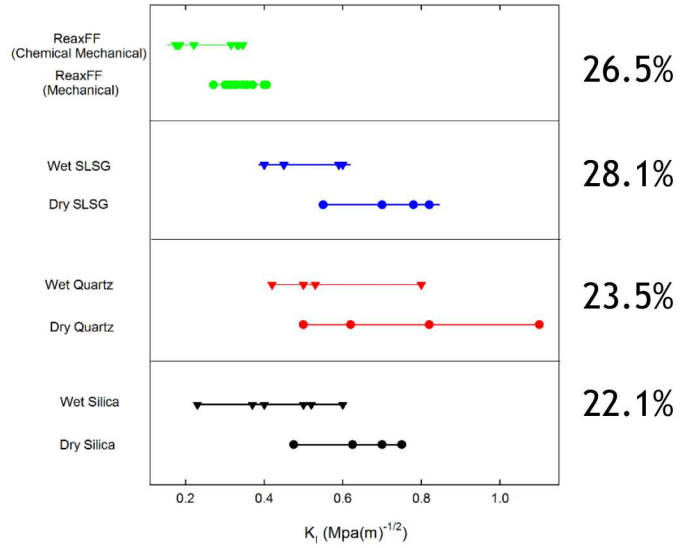


Experimental $K_{IC}$ data for amorphous silica, quartz, and soda-lime silicate glasses in dry and aqueous environments compared with current data.

# Stress Distributions

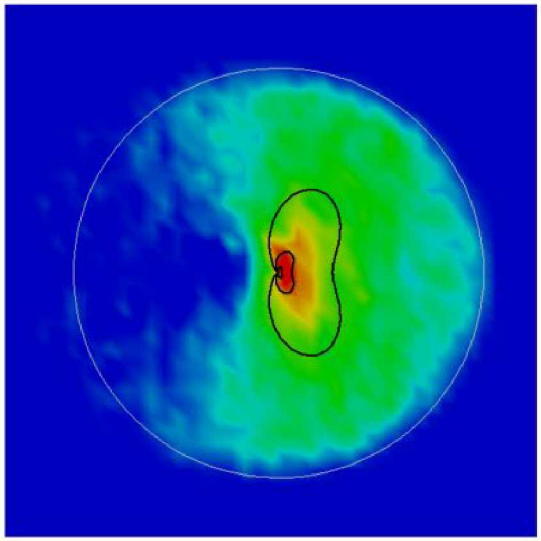

**Mechanical**
(mechanical loading only)

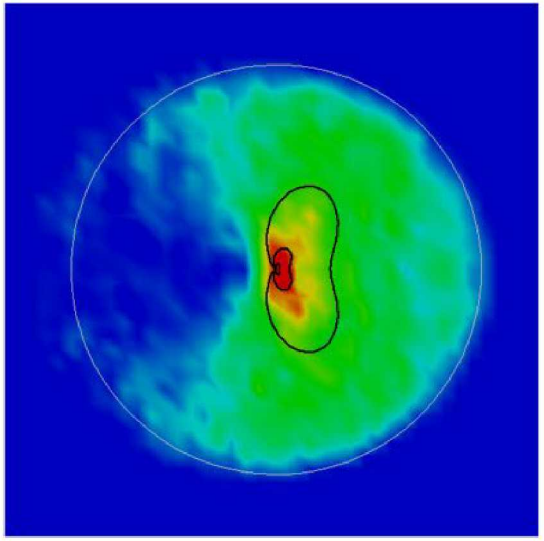

**Chemical-Mechanical**
(aqueous environment and mechanical loading)

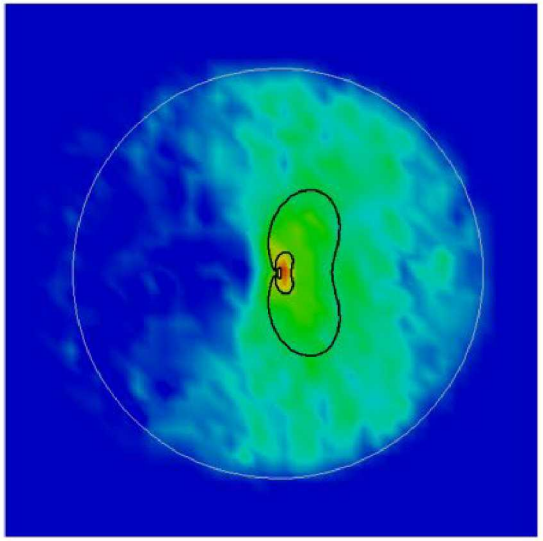

**Chemical**
(aqueous environment only)

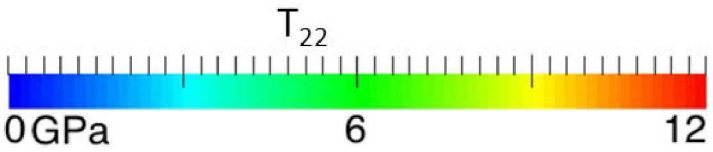


Stresses from the atomistic simulations were coarse grained to describe the stress states surrounding the fracture tip. Stress fields for silica systems in mechanical ($K_I$=0.2 MPa$\sqrt{m}$), chemical-mechanical ($K_I$=0.2 MPa$\sqrt{m}$), and chemical conditions ($K_I$=0.15 MPa$\sqrt{m}$).

# Fracture Propagation in Water

- Fracture depth identifies aggregate effect of aqueous environment on fracture
- Chemical-mechanical conditions: longer fracture propagation, larger number of fracture events and slightly shorter average fracture length
- Chemical effects become more prominent as the fracture propagates
- May be altering the conditions for fracture (bond stretching, stress states etc.)
- Chemical impact is more than additive on fracture growth

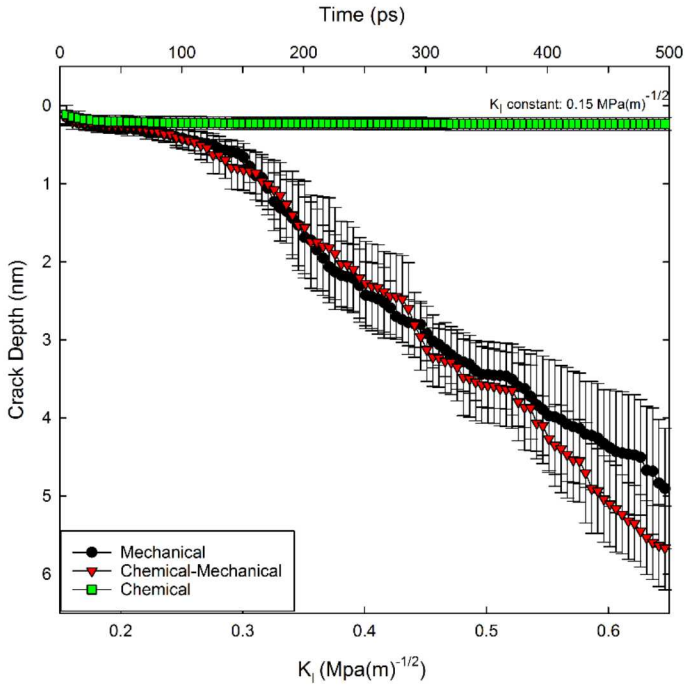


Crack depth for silica systems in mechanical, chemical, and chemical-mechanical conditions.

Crack propagation data for silica systems under different conditions.

| Conditions | Propagation (nm) | Fracture Events* (#) | Average Fracture Length (nm) | Longest Fracture (nm) | Fracture Velocity (m/s) |
|---|---|---|---|---|---|
| Mechanical | 4.92±0.76 | 11.50±2.06 | 0.35±0.08 | 0.90±0.23 | 9.85±1.51 |
| Chemical | 0.23±0.07 | 0.50±0.50 | 0.16±0.08 | 0.10±0.08 | 0.47±0.16 |
| Chemical-Mechanical | 5.69±0.53 | 14.83±2.41 | 0.32±0.06 | 0.97±0.38 | 11.38±1.07 |

# Silica Surface Sites in 1M NaCl and 1 M NaOH Solutions

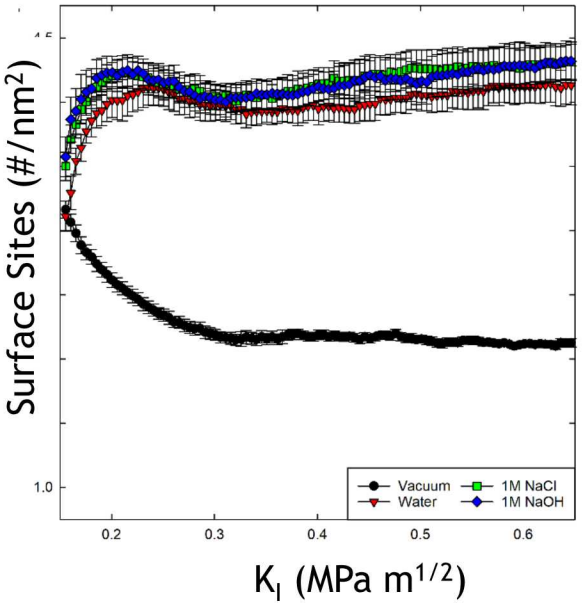


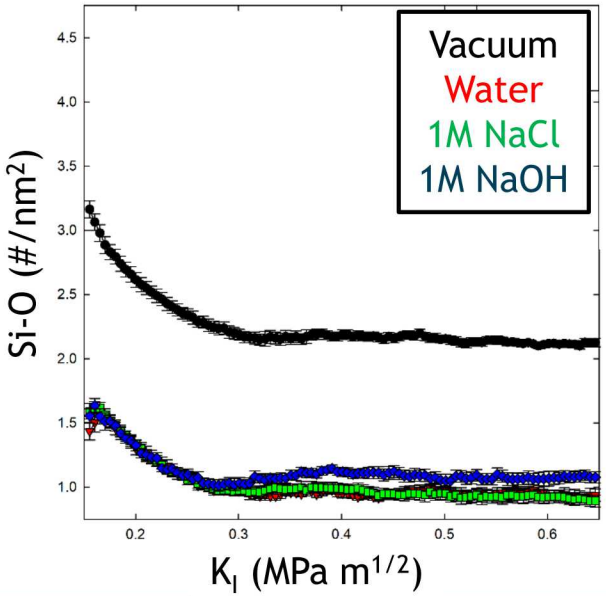


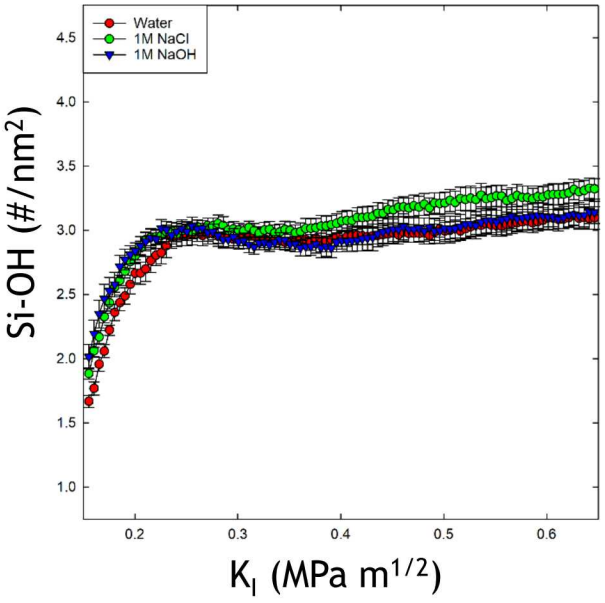


- In vacuum, there are no Si-OH surface sites.
- In vacuum, surface relaxation causes some surface sites to reconnect and form siloxane bonds.
- Silica surfaces exposed to salt solutions exhibit more surface sites than those in pure water suggesting a higher concentration of broken Si-O- bonds.
- More Si-OH sites form in 1M NaCl solutions; more $Si\text{-}O^-$ sites form in 1M NaOH solutions.

- Surface structure is influenced by solution composition.

# Solution Composition in Fracture

## $OH^-$ Concentration in Solution

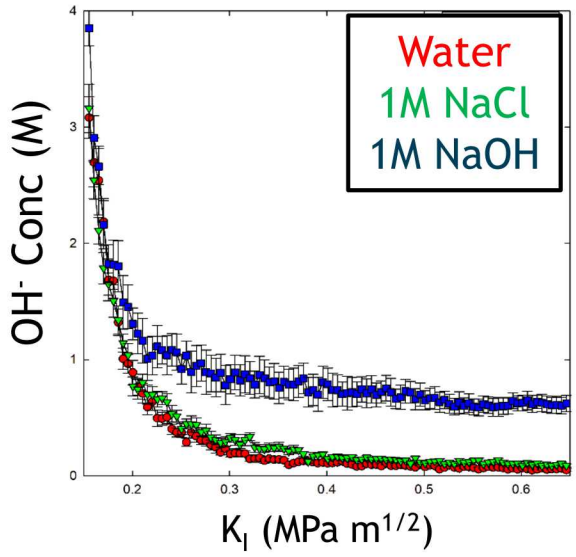


## $H_3O^+$ Concentration in Solution

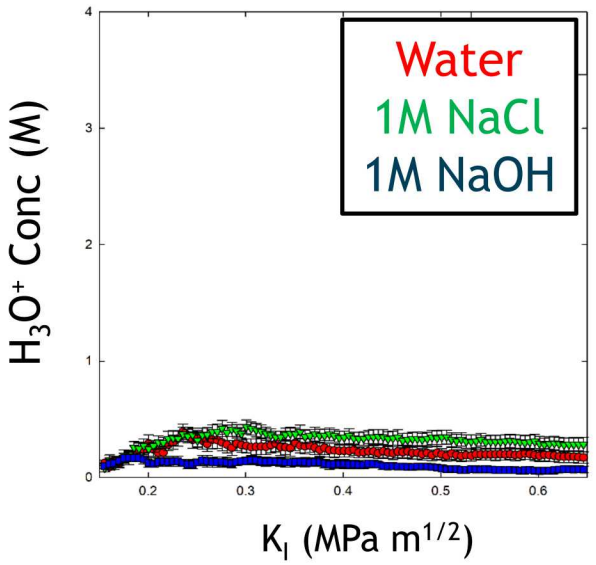


- Rapid change in concentrations occurs with initial loading before crack propagation
- Steady-state concentration occurs at ~0.25-0.3 MPa$\sqrt{m}$ due to balance of rate of water infiltration and addition of NaCl or NaOH molecules as fracture is loaded
- Concentration of $H_3O^+$ increases with decreasing pH: 1 M NaOH < water < 1 M NaCl.
- Silica dissolution should be higher in both NaCl and NaOH solutions than in pure water.

# Accessibility of Fracture Tip to Different Ions

Water

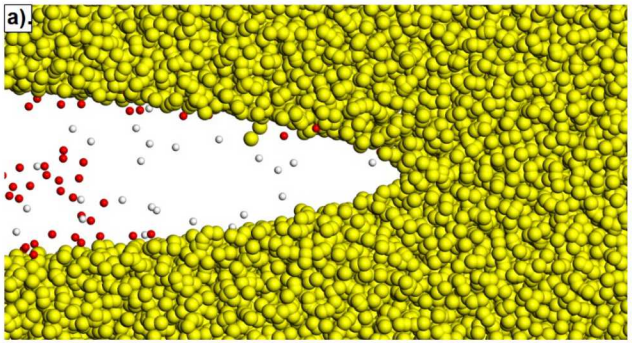


1M NaCl

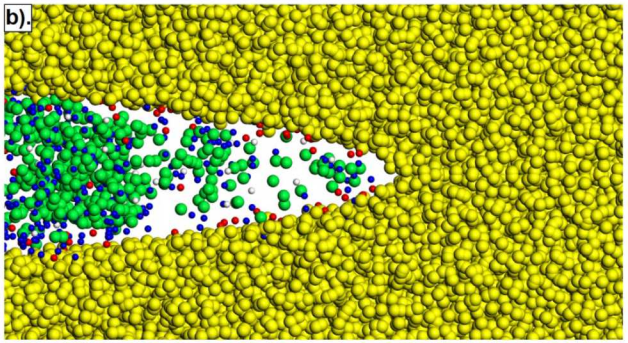


1M NaOH

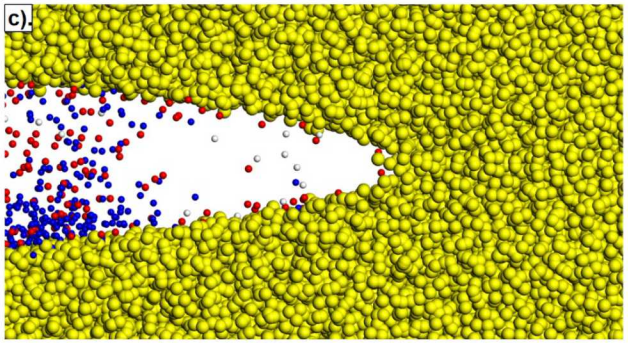


Si $H_3O^+$ $OH^-$ $Na^+$ $Cl^-$

- NaCl and NaOH molecules were added at the widest point in the fracture to emulate diffusion of ions from the bulk fluid
- For silica fracture in $H_2O$, the crack tip is filled with $H_2O$ and a few $H_3O^+$
- $OH^-$ migrates to fracture tip in both NaCl and NaOH solutions
- In NaCl solutions, the tip is filled with $Na^+$, $Cl^-$ and some $OH^-$, $H_3O^+$
- Limited $Na^+$ diffusion into crack tip from NaOH solution; crack tip contains surface coordinated $OH^-$ or free $H_3O^+$.

# $Na^+$ Coordination Structures

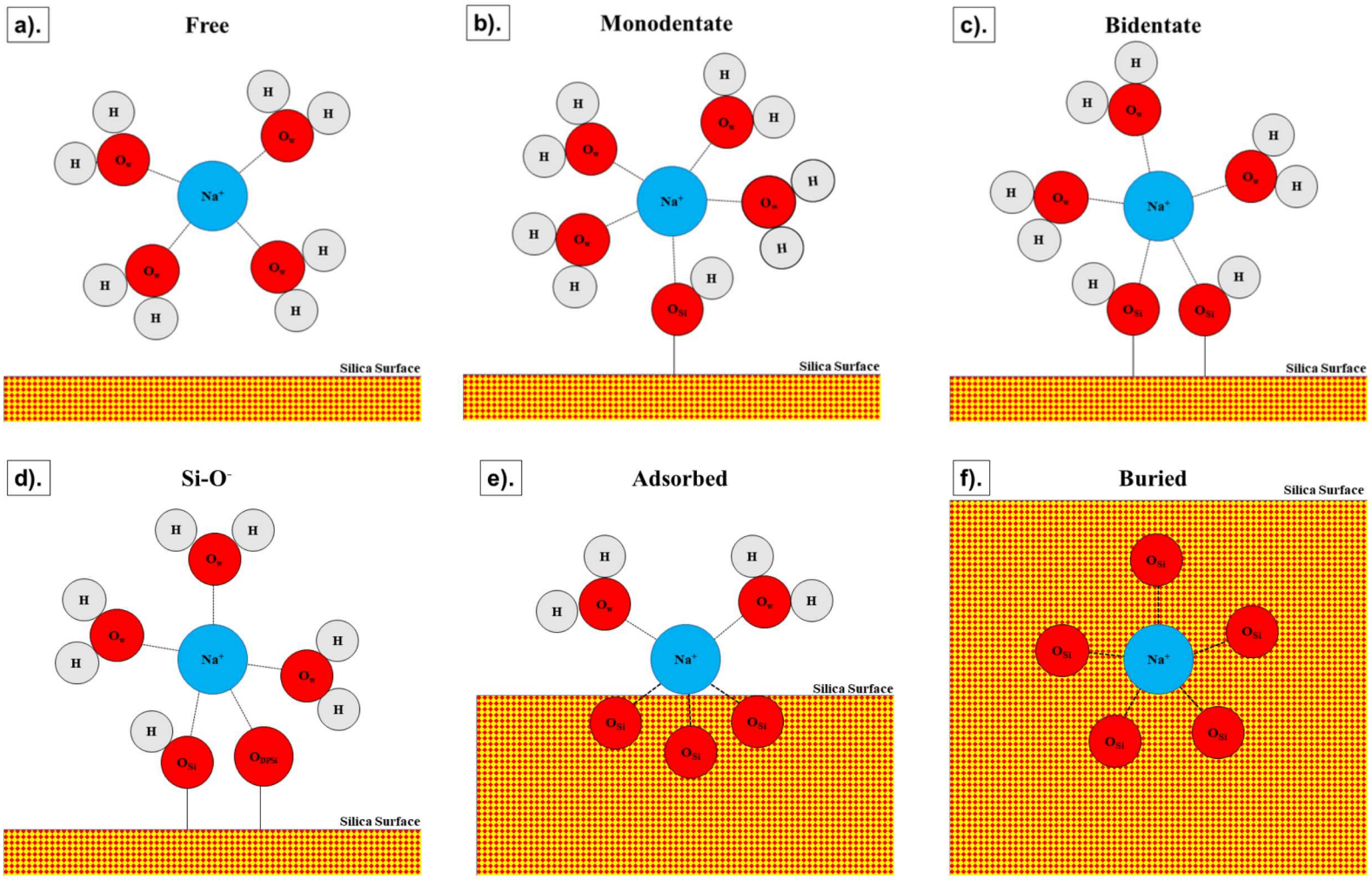


Structure (d) does not occur on flat surfaces: nanoconfinement effect of fracture tip

# Fracture Properties of Silica for Different Environmental Conditions

| | $eK_{IC}$ (MPa√m) | | Fracture Events (#) | $G_{IC}$ (J/m²) | $G_{diss}$ (J/m²) | Si-OH (#/nm²) | γ (J/m²) |
|---|---|---|---|---|---|---|---|
| | First | Average | | | | | |
| Vacuum | 0.34±0.04 | 0.43±0.04 | 3.67±1.18 | 7.91 | 6.78 | 0.00 | 1.13 |
| Water | 0.20±0.06 | 0.37±0.05 | 4.33±1.03 | 4.59 | 4.21 | 3.10 | 0.38 |
| 1M NaCl | 0.28±0.09 | 0.41±0.05 | 5.42±1.66 | 5.14 | 4.75 | 3.04 | 0.39 |
| 1M NaOH | 0.19±0.05 | 0.37±0.05 | 6.00±1.41 | 5.47 | 5.06 | 2.95 | 0.41 |

## Ranking of factors that influence environmentally assisted fracture

| | $eK^*_{IC}$ | Fracture events | Dissolution | $Si\text{-}O^-$ # | Tip access | Radius of curvature |
|---|---|---|---|---|---|---|
| Water | 2 | 3 | 3 | 3 | 3 | 3 |
| 1M NaCl | 1 | 2 | 1 | 2 | 1 | 1 |
| 1M NaOH | 3 | 1 | 2 | 1 | 2 | 2 |

# Conclusions

- Amorphous silica is substantially weaker when in contact with aqueous solutions than in vacuum due to chemical reactions with preexisting cracks.
- Fracture toughness is lowest for silica in 1M NaOH solutions. The basic solution leads to higher surface deprotonation, less dissolution, and a narrower radius of curvature than in an acidic environment.
- The 1M NaCl solution causes more silica dissolution than pure water or a 1M NaOH solution and changes the geometry of the fracture tip. In addition $Q^0$ silica species are observed in solution.
- The nanoconfinement at the fracture tip results in different $Na^+$ adsorption mechanisms than on a flat surface.

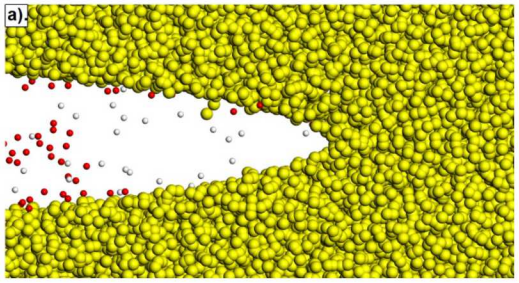


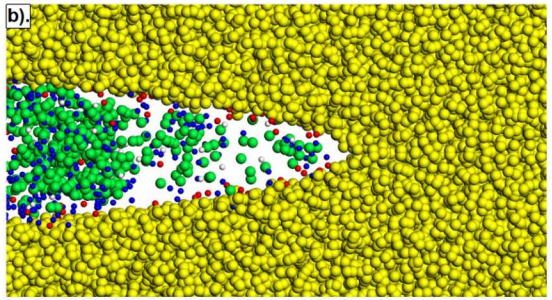


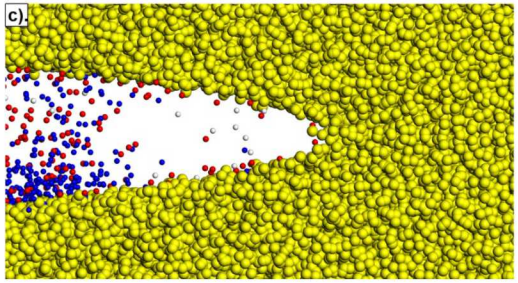


This work was fully supported by the Laboratory Directed Research and Development (LDRD) program of Sandia National Laboratories.

# Energy Dissipation

- G is related to both the surface energy and dissipative energy (unrecoverable inelastic character around the fracture tip)

$$G = G_{diss} + 2\gamma_s$$

- $G_{diss}$ is calculated from energy and surface area of the fracture:

$$\frac{\Delta U}{\Delta S_A} = G_{diss}$$

  - Surface energy (γ) = related to hydroxylation of the surface
  - Wet fracture results in a lower $K_{IC}$ value and lower $G_{IC}$, due to larger dissipation energy
  - Larger $G_{diss}$ relates to the strain distribution surrounding the fracture tip

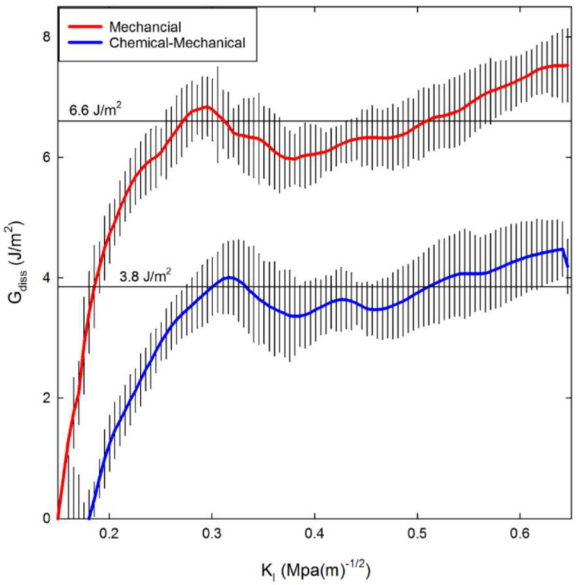


**Energy dissipation ($G_{diss}$) during crack loading and subsequent crack propagation for silica systems**

Fracture properties of silica in mechanical and chemical-mechanical conditions.

| | $K_{IC}$ (MPa√m) | $G_{IC}$ (J/m²) | $G_{diss}$ (J/m²) | Si-OH (#/nm²) | γ (J/m²) |
|---|---|---|---|---|---|
| Mechanical | 0.339±0.037 | 8.8 | 6.6 | 0.0 | 1.1 |
| Chemical-Mechanical | 0.246±0.074 | 4.6 | 3.8 | 3.1 | 0.4 |